Molecular and Cellular Endocrinology 604 (2025) 112553

Contents lists available at ScienceDirect

Molecular and Cellular Endocrinology

journal homepage: www.elsevier.com/locate/mce

Pleiotropic signaling of single-chain thyrostimulin (GPB5-GPA2) on homologous glycoprotein hormone receptors (ScFSHR, ScLHR, ScTSHR) in the elasmobranch *Scyliorhinus canicula* reproduction

Fabian Jeanne [a], Stanislas Pilet [a], Yves Combarnous [b], Benoît Bernay [c], Sylvie Dufour [d], Pascal Favrel [a], Pascal Sourdaine [a,*]

[a] Université de Caen Normandie, Marine Ecosystems and Organisms Research lab (MERSEA), UR 7482, 14032, Caen, cedex 5, France
[b] INRAE, CNRS, Université de Tours, UMR Physiologie de la Reproduction & des Comportements, 37380, Nouzilly, France
[c] Université de Caen Normandie - Plateforme PROTEOGEN, US EMerode, 14032, Caen, cedex 5, France
[d] Muséum National d'Histoire Naturelle (MNHN), UCN, SU, UA, CNRS, IRD, Laboratoire de Biologie des Organismes et Ecosystèmes Aquatiques (BOREA), UMR 8067, 43, rue Cuvier, CP 26, 75231, Paris, Cedex 05, France

ARTICLE INFO

Keywords:
Thyrostimulin
GPA2
GPB5
TSH
Testis
Epididymis
Elasmobranchs

ABSTRACT

The pituitary glycoprotein hormones (GPHs) control several physiological processes in vertebrates such as reproduction and metabolism. They include the luteinizing hormone (LH), the follicle-stimulating hormone (FSH), and the thyroid-stimulating hormone (TSH), which activate their cognate leucine-rich repeat G protein-coupled receptors (LGRs), LHR, FSHR, and TSHR. Each GPH consists of a common α subunit and a specific βFSH, βLH or βTSH subunit. More recently, two supplementary GPH proteins, GPA and GPB, were identified in nearly all bilaterians and are the ancestors of the pituitary GPH α- and β-subunits, respectively. Chondrichthyans (holocephalans and elasmobranchs), the sister group of bony vertebrates, are the most ancient clade to possess diversified GPH subunits. In the present study, GPA2, GPB5, TSHβ2, but not TSHβ1, and TSHR sequences have been identified in several elasmobranch genomes, and their 3D models were analyzed. Functional hormone-receptor interactions were studied in the small-spotted catshark (*Scyliorhinus canicula*) and showed that conditioned media from cells expressing the recombinant single-chain *Sc*GPB5-*Sc*GPA2 were more effective than independent subunits in activating *Sc*TSHR, *Sc*FSHR, and *Sc*LHR. Expression profiles were analyzed by real-time PCR, *in situ* hybridization, and immunohistochemistry along the male genital tract, other male and female tissues, and female tissues. A broader tissue distribution expression was observed for *tshr* and *gpa2* than for *gpb5,* which was mainly observed in the testes. In testis, expression of *tshr* and *gpb5* by Sertoli cells and of *gpa2* by germ cells suggested paracrine/autocrine functions of GPA2/GPB5/GPHR signaling during spermatogenesis. This study complements the data on GPA2 and GPB5 by studying a chondrichthyan of phylogenetic interest for understanding the evolution of endocrine regulation in vertebrates.

1. Introduction

Glycoprotein hormones (GPHs) belong to the family of cystine-knot proteins and exert a wide range of physiological functions by activating their cognate leucine-rich repeat-containing G protein-coupled receptors (LGRs). In mammals, pituitary GPHs comprise two gonadotropins (GTHs), follicle-stimulating hormone (FSH) and luteinizing hormone (LH), as well as thyroid-stimulating hormone (TSH) also named thyrotropin. The pituitary GPHs comprise a common α-subunit (CGA) and a specific β-subunit (FSHβ, LHβ, TSHβ), forming non-covalent heterodimers. FSH and LH are produced by the anterior pituitary, under the regulation of hypothalamic gonadotropin-releasing hormone (GnRH) signaling, and regulate gonadal functions by interacting with their receptors, FSHR and LHR, thus constituting the hypothalamic-pituitary-gonadal (HPG) axis. The pituitary TSH is regulated by the hypothalamic thyrotropin-releasing hormone (TRH) and regulates thyroid function by interacting with its receptor, TSHR, thus forming the hypothalamic-pituitary-thyroid (HPT) axis. These GPH subunits, with their cognate receptors, emerged before the gnathostome radiation (Heyland et al., 2012; Roch and Sherwood, 2014).

* Corresponding author.
E-mail address: pascal.sourdaine@unicaen.fr (P. Sourdaine).

https://doi.org/10.1016/j.mce.2025.112553
Received 23 January 2025; Received in revised form 24 March 2025; Accepted 17 April 2025
Available online 18 April 2025

The β-subunits derived from an ancestral gene (*gpb*) through the two whole genome duplications, 1R and 2R, generating two gonadotropin β subunits, *lhβ* and *fshβ*, as well as two thyrotropin β subunits, *tshβ1*, and *tshβ2*, present in some chondrichthyes, the holocephalan *Callorhinchus milii* and the batoidea *Leucoraja erinacea*, and in early lobe-finned fish, the coelacanth *Latimeria chalumnae* and the lungfish *Neoceratodus forsteri*, while *tshβ2* was lost in actinopterygians and tetrapods (Dufour et al., 2020; Maugars et al., 2014; Querat, 2021). In the early 2000s, two supplementary GPH subunit-related genes, *gpa2,* and *gpb5*, were identified from the human genome (Hsu et al., 2002). The ability of recombinant cross-linked hGPA2#hGPB5 heterodimer to activate TSHR in *Homo sapiens* and *Ratus norvegicus* led to call the corresponding GPH as Thyrostimulin, but also referred to as Corticotroph-derived glycoprotein hormone (CGH) (Nagasaki et al., 2006; Nakabayashi et al., 2002). *Gpa2* and *gpb5* orthologs were identified in almost all animal species including protostomia (Heyland et al., 2012; Kudo et al., 2000; Sudo et al., 2005; Wahl et al., 2022), primitive chordates (Dong et al., 2013; Wang et al., 2018; Yang et al., 2023), cyclostomata (Sower et al., 2015) and various vertebrates (Buechi and Bridgham, 2017; Cahoreau et al., 2015; Hara et al., 2018; Levavi-Sivan et al., 2010) but not in cnidaria (Dos Santos et al., 2009). Molecular ancestors of GPHRs have also been identified under various names and can be activated by recombinant GPA2/GPB5 and GPA2#GPB5 heterodimers or recombinant single-chain GPB5-GPA2 proteins. Such GPHRs were identified in protostomia (Kenis et al., 2023; Rocco and Paluzzi, 2020; Sudo et al., 2005; Wang et al., 2018), primitive chordates (Dos Santos et al., 2009; Wang et al., 2018; Yang et al., 2023) and cyclostomata (Hausken et al., 2018); highlighting the coevolution of the GPH with GPHR signaling along bilateria evolution. However, the question of whether GPA2 and GPB5 are active *in vivo* as non-covalent heterodimers, homodimers, or monomers has been raised. Indeed, the absence of a seatbelt in GPB5, as well as the expression of GPA2 and GPB5 essentially in different cells, are not in favor of dimerization (Alvarez et al., 2009; Dufour et al., 2020; Yang et al., 2023). Concerning the GPA2/GPB5 heterodimer (thyrostimulin), it would be involved in several biological functions through the activation of TSHR, in addition to regulating thyroxine production (Nagasaki et al., 2006; Nakabayashi et al., 2002), such as bone formation (Bassett et al., 2015), immune response (Suzuki et al., 2009) and reproduction (Sun et al., 2010) in mammals, as well as development in protostomes (Heyland et al., 2012; Vandersmissen et al., 2014). The role of GPA2/GPB5 in reproduction has been highlighted in *H. sapiens* as a paracrine factor secreted by the oocyte and activating granulosa and theca cells which express TSHR (Sun et al., 2010). In males, the role of thyrostimulin has been demonstrated in studies using RNAi down expression of the GPHR of protostomia such as in the nematode, *Caenorhabditis elegans*, where down expression of its FSHR-1 results in the absence of germ cell renewal (Cho et al., 2007) and in the mosquito, *Aedes aegypti,* where down expression of its LGR1 results in abnormal spermatogenesis (Rocco et al., 2017, 2019). In addition, *gpa2*, *gpb5,* and their cognate receptor genes are coexpressed in the gonads of several protostomia such as the fly, *Drosophila melanogaster* (Vandersmissen et al., 2014), the scallop, *Patinopecten yessoensis* (Zhang et al., 2020) and the prawn, *Macrobrachium rosenbergii* (Wahl et al., 2022). They are also coexpressed in the gonads of Chordata, such as the amphioxus, *Branchiostoma japonicum* (Wang et al., 2018), the ascidian, *Styela clava* (Yang et al., 2023), the lamprey, *Petromyzon marinus* (Hausken et al., 2018) and the catshark, *Scyliorhinus torazame* (Hara et al., 2018).

The study of the GPA2/GPB5 signaling in chondrichthyes is of interest because of their unique phylogenetic position. Indeed, the chondrichthyes are the sister group to osteichthyes (bony vertebrates), whose divergence occurred around 450 million years ago (Irisarri et al., 2017), and include the holocephalans (chimaeras) and elasmobranchs (sharks and rays). In terms of the comparative evolution of HPG and HPT endocrine axes, chondrichthyes illustrate the first representatives of jawed vertebrates with specialized HPG and HPT axes, located between on the one hand, cyclostomata, which might have non-differentiated HPG and HPT axes with two GPHs (lGpH and inferred thyrostimulin) and two GPHRs (lGpH-R I and –R II) (Sower and Hausken, 2017), and on the other hand, the bony vertebrates. The first study to examine the specificity of interactions between GPHs and GPHRs in a chondrichthyan was carried out on the holocephalan *C. milii*. It showed high specificity for FSH/FSHR, LH/LHR, and TSH/TSHR complexes, while recombinant GPB5-GPA2 activated none of the GPHRs (Buechi and Bridgham, 2017). However, the GPA2 and GPB5 signalings remain to be characterized in elasmobranchs which diverged as early as 380 million years ago from holocephalans. Interestingly, Hara's work, based on a global genome expression analysis of the shark *S. torazame*, showed that *gpa2* was expressed in multiple tissues, including the testis, whereas *gpb5* expression appeared to be restricted to the testis (Hara et al., 2018). This result motivated us to develop a more comprehensive study during spermatogenesis in another chondrichthyan, the small-spotted catshark *Scyliorhinus canicula*, a nonendangered species belonging to the carcharhiniforms, which is the largest family of sharks.

Spermatogenesis is a highly conserved and orderly process under endocrine and paracrine regulations that allows the transformation of undifferentiated spermatogonia into spermatozoa. The testis of the small-spotted catshark *S. canicula* consists of spermatocysts (cysts), each made of spermatoblasts in which one Sertoli cell is associated with synchronously developing germ cells. On a cross-section of the testis, cysts originate from the germinative area, located on the dorsolateral edge of the testis. As new cysts are continuously formed, older cysts are moved to the opposite edge of the testis, leading to a zonal arrangement of cysts according to the spermatogenic wave. Thus, at least five testicular zones corresponding to the germinative area, the cysts with spermatogonia, the cysts with primary and secondary spermatocytes, the cysts with early spermatids, and the cysts with late spermatids, are easily distinguishable and accessible (Loir and Sourdaine, 1994). Another particularity of the *S. canicula* testis, also observed in another shark, *Squalus acanthias*, is the absence of differentiated Leydig cells, Sertoli cells being the main testicular steroidogenic cells (Cuevas and Callard, 1992; Pudney and Callard, 1984a, 1984b; Pudney and Callard, 1984b; Sourdaine and Garnier, 1993).

The present study aimed to complete the identification of GPA2, GPB5, TSHβ and TSHR proteins in several chondrichthyes and to analyze their structures and expression profiles by real-time PCR and *in situ* detections along spermatogenesis stages as well as in other tissues, including the male and female genital tracts of the small spotted catshark *S. canicula*. Using in vitro bioassays, specificities of hormone and receptor interactions were analyzed with *Sc*GPA2, *Sc*GPB5, and *Sc*TSHβ as single-chain recombinant heterodimers or monomers as ligands, and with the recombinant receptors *Sc*TSHR, *Sc*FSHR, and *Sc*LHR expressed in HEK293 cells for testing their respective activities. The results are discussed in an evolutionary perspective.

2. Materials and methods

2.1. Animals and tissue sampling

The catshark *S. canicula* was assessed, in 2020, as a least concern in the red list of threatened species by the IUCN (International Union for Conservation of Nature). Adult male (608 ± 137 g; 58 ± 3 cm) and adult female (647 ± 90 g; 57 ± 4 cm) catsharks were fished during a CGFS (Channel Ground Fish Survey) campaign by IFREMER in the East Manche in September 2022 (Giraldo et al., 2022). The animals were maintained in natural seawater tanks at the marine station of the University of Caen Normandy (*Centre de Recherches en Environnement Côtier* (CREC), Luc-sur-Mer, France). Under the A14384001 number, CREC facilities are approved by the Council Department of Population Care (Préfecture du Calvados, France). Sharks were acclimated 2 weeks before killing by percussive blow to the head followed by sectioning and pithing of the spinal cord and exsanguination according to the European directive 2010/63/UE. Testes, epigonal tissues, proximal and distal

epididymis, seminal ampullae, myelencephalons, cerebellum, midbrains/pituitaries, forebrains, olfactory bulbs, eyes, thyroid glands, Leydig organs, spleens, livers, pancreas, duodenums, kidneys, rectal glands, gills, hearts and muscles were sampled from 14 males and myelencephalons, cerebellum, middle part of the brain corresponding to diencephalon and mesencephalon and including pituitaries (Middle-brain/pituitary), forebrains, olfactory bulbs, ovaries, nidamental glands, oviducts, uterus and thyroid glands from 7 females and were transferred directly into liquid nitrogen before storage at −80 °C with the exception of testes which were transferred in ice-cold Gautron's buffer (pH 7.8, 890 mosmol kg-1) (Gautron, 1978) with 58 mM trimethylamine-N-oxide (TMAO, Sigma, 317594) before dissection into the four zones (Loir and Sourdaine, 1994) corresponding to the zone containing the germinative area and cysts with spermatogonia (zone A), cysts with spermatocytes (zone B), cysts with early spermatids (zone C) and cysts with late spermatids (zone D). Other tissues such as testes, epididymis heads and bodies, ovaries, brains, thyroid glands, and Leydig's gland were fixed in Gautron's buffer with paraformaldehyde 4 % before alcoholic dehydration and stocked in butan-1-ol at −20 °C.

2.2. Sequence searches

GPA2, GBP5, TSHβ and TSHR amino acid sequences were identified using BLAST searches, based on *C. milii* sequences (Buechi and Bridgham, 2017) against the following genomes and databases: *Amblyraja radiata* (sAmbRad1.1.pri), *Carcharodon carcharias* (Marra et al., 2019), *Chiloscyllium plagiosum* (ASM401019v1), *Chiloscyllium punctatum* (Hara et al., 2018), *Pristis pectinata* (sPriPec2.1.pri), *Rhincodon typus* (Read et al., 2017), *S. canicula* (sScyCan1.2) and *S. torazame* (Hara et al., 2018) on NCBI (https://www.ncbi.nlm.nih.gov/genome/); of *Hemitrygon akajei* (sHemAka1.1) on Squalomix Blast Server (https://transcriptome.riken.jp/squalomix/blast/); and of *L. erinacea* (Wang et al., 2012) on Skatebase (http://skatebase.org). To verify the relationship between obtained sequences and their putative families, phylogenetic trees were built based on the previous work of Buechi and Bridgham (2017) using the MAFFT (Multiple Alignment using Fast Fourier Transform) program, BMGE (Block Mapping and Gathering with Entropy) alignment curation and PhylML tree inference on NGPhylogeny online services (https://ngphylogeny.fr/workflows/oneclick/ (Lemoine et al., 2019), with a bootstrap of 1000. Sequences used are listed (Supplementary Data, Excel). Obtained trees were finalized using iTOL online tool (https://itol.embl.de/, (Letunic and Bork, 2021).

Synteny analyses of vertebrate *gpa2*, *gpb5*, *tshβ1*, and *tshβ2* genomic regions were performed to annotate the orthologs identified in the batoid *A. radiata* and the sharks *S. canicula* and *C. carcharias*. Species occupying key phylogenetic positions were selected, including the cyclostome *P. marinus*, the chondrichthyan *C. milii*, the actinopterygian *L. oculatus*, and the sarcopterygians *L. chalumnae*, *X. laevis* and *H. sapiens*. Genomic regions of *C. milii* were selected as templates. The genes were mapped using NCBI's Genome Data Viewer (https://www.ncbi.nlm.nih.gov/genome/gdv/) and, for unretrieved genes, tBlastn using orthologous protein sequences were performed.

2.3. D model building

Multiple alignments were performed using the Clustal Omega package (https://www.ebi.ac.uk/Tools/msa/clustalo/ (Sievers et al., 2011),) with manual corrections to identify conserved structures (based on the knowledge in *H. sapiens* sequences). Signal peptides were predicted using predisi software (http://www.predisi.de/). Predictive models of GPA2s, GPB5s, TSHβs and TSHRs were built using SWISS-MODEL (https://swissmodel.expasy.org/, (Waterhouse et al., 2018), using the Q96T91.1.A, Q86YW7.1.A and the 7utz.1 template of *H. sapiens*, and finalized using the Swiss PDB Viewer program (Johansson et al., 2012). Obtained models were evaluated by retaining the global sequence identities against the template, the greatest GMQE score (Global Model Quality Estimate, Waterhouse et al., 2018), which depends on coverage, and the highest QMEANDisCo Global score (Studer et al., 2020), which evaluates the model 'as is' without explicit coverage. The same procedure was performed with *H. sapiens* sequences, as control, and for *C. milii* sequences. Using Swiss-PdbViewer (Johansson et al., 2012), predicted models were superimposed and the Root Mean Square Deviation (RMSD) was calculated and averaged for each GPH subunit and GPHRs.

2.4. Functional hormone-receptor interaction in in vitro assays

Synthetic pTarget plasmids containing *S. canicula* cDNA sequences for *fshr* (*Sc-fshr*), *lhr* (*Sc-lhr*) or *tshr* (*Sc-tshr*) were obtained from Twist Bioscience (San Francisco, USA) and synthetic pTarget plasmids containing the fusion constructs *Sctshβ-Sccga* and *Scgpb5-Scgpa2* were obtained from GenScript Biotech (Rijswijk, Netherlands), in addition to pTarget plasmids containing the *Scgpa2* alone or the *Scgpb5* alone. Human embryonic kidney (HEK293T) cells, chosen for their lack of glycoprotein hormone receptor expression (Atwood et al., 2011), were transiently transfected with the synthetic plasmid using FuGENE HD (Promega) according to the manufacturer's instructions. Cotransfection of a *gphr*/pTarget construct and a pTarget expression construct for the human $G\alpha_{16}$ subunit was performed to get a measurable response. $G\alpha_{16}$ can direct intracellular signaling of all GPCRs towards calcium release *via* the phospholipase Cβ pathway, regardless of the endogenous G protein coupling of the receptor. The pTarget ligand constructs were transfected in HEK293T cells around 80 % of confluence in 75 cm^2 flasks, then after 24 h of culture, the media were collected and concentrated using Amicon® 3K filters (Millipore). As a negative control, HEK293T cells were transfected with empty pTarget only or Gα16 together with empty pTarget to verify that native HEK293T cells were not stimulated by single-chain *Sc*-TSHB-CGA, *Sc*-GPB5-GPA2, *Sc*-GPA2 or *Sc*-GPB5 treatments. Activation of the *S. canicula* GPHRs by these molecules was monitored using a fluorescence-based calcium mobilization assay according to Schwartz et al. (2021). Briefly, transfected HEK293T cells were loaded with Fluo-4 Direct (Invitrogen) for 1 day at 37 °C with 5 % of CO_2. The fluorophore was excited at 488 nm. The calcium-dependent emission was measured at 525 nm for 2 min using a Flexstation 3 (Molecular Devices) at 37 °C and analyzed using SoftMax Pro (Molecular Devices). For analysis of the activation of the Gαs/adenylyl cyclase/cAMP/PKA pathway, transfected cells were incubated with Glosensor cAMP reagent (4 % final concentration in media) (Promega) for 2 h at room temperature before the injection of the ligand (*Sc*-TSHB-CGA, *Sc*-GPB5-GPA2, *Sc*-GPA2 or *Sc*-GPB5) and cAMP luminescence response was measured at 37 °C for 30 min using the Flexstation 3.

To determine the absolute concentrations of the ligands produced, an initial proteomic analysis of the ligand-containing media was carried out using high-resolution nanoLC-ESI-MS/MS to identify peptides resulting from trypsin digestion of the α-subunit (*Sc*CGA), *Sc*GPA2 and *Sc*GPB5. The VTLMGNLK, EEIEIFTAK, and EFTFLAK peptides were designed for *Sc*CGA, *Sc*GPA2 and *Sc*GPB5, respectively, according to the following criteria: the absence of cysteine residue, the absence of post-translational modifications, and more than 5 amino-acids. Selected peptides were synthesized by CliniSciences (Nanterre, France) and used as internal quantity markers. The standard curves were established, ranging from 16.3 pg/µl to 666 pg/µl, and the equations obtained were $y = 400.05x-6339.1$ ($R^2 = 0.9967$), $y = 979.22x-3058.1$.

($R^2 = 0.9997$) and $y = 231.1x+11558$ ($R^2 = 0.9747$) for *Sc*CGA, *Sc*GPB5, and *Sc*GPA2, respectively, where "y" was the peak area of the peptide and "x" was the concentration. Efficiency (EC_{50}) and efficacy (Emax) were calculated with 95 % confidence intervals (profile likelihood) from sigmoidal dose-response equations which were constructed with a nonlinear regression analysis using Prism 5.0 (GraphPad Software, USA).

2.5. Reverse transcription and RT-qPCR

Total RNAs were extracted from *S. canicula* tissues using Tri-Reagent (Sigma-Aldrich, 93289) before purification with the NucleoSpin RNAII columns kit (Machery-Nagel). They were quantified with a NanoDrop™ 2000 (Thermo Scientific) and degradation analyses were performed with an Agilent 2100 Bioanalyzer (Agilent) for testes zones, epigonal tissues, male brains and ovaries. Obtained RNA integrity numbers were greater than 7. For tissue distribution, real-time PCR was performed independently for three animals (N = 3) in triplicate (n = 3) except for testes (zone A, B, C, and D) and epigonal tissue where six animals were used (N = 6, n = 18). The CFX Connect Detection System (Bio-Rad) was used for RT-qPCR analyses. Two hundred and seventy ng of total RNAs were treated with 1U of RQ1 DNase (Promega, M6101) (37 °C/20min) following by the reverse transcription using 1 ng random hexanucleotide primers (Promega, C1181), 0.5 mM dNTPs and 200 U of M-MLV Reverse Transcriptase (Promega, M1701) then the reactions were stopped (70 °C/5min). The gene-specific primers (Supplementary Table S1) were designed using Primer-BLAST (https://www.ncbi.nlm.nih.gov/tools/primer-blast/ (Ye et al., 2012), with manual corrections according to the following criteria: length between 18 and 22 bp, GC content over 50 %, Tm close to 60 °C and generation of a 150–200 bp amplicon. The real-time PCR (5 ng of cDNA, 40 cycles: 95 °C/15s, 60 °C/45s) was done with the GoTaq®qPCR Master Mix (Promega, A6001). Melt curve analysis and efficiency tests were carried out to ensure the primers amplified a single product with 90–110 % efficiency. The Ct values were read at 200 relative fluorescence units and normalized against the 5S RNA (Redon et al., 2010) using the ΔC_t method (Schefe et al., 2006). The $2^{-\Delta\Delta Ct}$ method (Livak and Schmittgen, 2001) allowed us to calculate the expression variations based on the mean ΔC_t of all tissues. Comparison of the Ct 5SRNA/total RNA ratio between tissues showed no significant difference using the non-parametric Kruskal-Wallis test with a P-value of 0.14 (Supplementary Fig. S1). Statistical analyses were performed using a first Shapiro-Wilk test analysis followed by the non-parametric Mann-Whitney *U* test for P-value <0.05.

2.6. In situ hybridization

Digoxigenin-conjugated riboprobes were synthesized from cDNA clones produced with specific primers (Supplementary Table S2). The resulting amplicons were cloned in pCR™II-TOPO™ Vector by TA cloning and then transformed into chemically competent *E. coli* using the TOPO TA Cloning kit (Invitrogen, k461020). After cultures, plasmids were purified using the Wizard® Plus SV Minipreps (Promega, A1340) then the digoxigenin-conjugated riboprobes were generated using M13 PCR on 100 ng of plasmids with 1 mM $MgCl_2$, 0.2 mM of each dNTP, 0.4 µM M13 primer and 0.625 U GoTaq® Flexi DNA Polymerase (Promega, M8291). The cycling parameters were as follows: 1X(95 °C, 5min), 30X [(95 °C, 30s), (60 °C, 45s), (72 °C, 1min30s)], 1X(72 °C, 5min). PCR products were quantified using a Nanodrop 2000 spectrophotometer (Thermo Scientific) and then purified using the NucleoSpin RNA Clean-up (Marcherey-Nagel, 740948.50). The size checking was done using gel migration. *In vitro* transcriptions were carried out for 3 h at 37 °C on 1.2 µg PCR products with 25 U RNAsin, 25 U T7 or SP6 polymerase, 10 mM dithiothreitol, 1 mM rATP, rCTP and rGTP, 0.65 mM rUTP, and 0.35 mM digoxigenin-UTP (Roche, 03359247910) using the Riboprobe® Combination Systems (Promega, P1460). DNAs were digested with 2 U RQ1 DNAse (Promega, M6101) for 30 min at 37 °C. The riboprobes obtained were purified and their qualities were checked by dot blots on PVDF membrane. Paraffin slices (5 µm) were incubated at 61 °C to facilitate deparaffinization using Roti-histol (sigma, 6640.6). Hydration was achieved by successive ethanol baths (100 %, 95 % and 70 %), then by PBS. Slices were treated with 4 % PFA in PBS, with 5 µg/ml proteinase k in Tris buffer for 4 min, with 4 % PFA in PBS, with 100 mM triethanolamine in 25 % acetic acid, then with 100 mM glycine in Tris buffer with PBS washes between each treatment. Tissues were incubated for 1 h at 65 °C with the hybridization mix (50 % deionized formamide, 1X saline-sodium citrate (SSC), 0.5 M ethylenediaminetetraacetic acid (EDTA), 10 % Tween 20, 1X Denhardt'solution, 28 mg/ml dextran sulfate, 0.1 mg/ml heparin, 10 % CHAPS, 0.5 mg/ml tRNA). Then, 0.1–0.4 ng/µl riboprobes in the hybridization mix were incubated overnight at 65 °C. Slices were washed using successive baths of diluted SSC 20X (SSC 1X and SSC 1.5X at 65 °C, SSC 2X at 37 °C, SSC 2X with 0.2 µg/ml of RNase A (Promega, A797C) at 37 °C, and SSC 0.2X at 60 °C) followed by maleic acid buffer baths with 0.3 % Triton (MABT). For immunostaining and revelation, the DIG Nucleic Acid Detection kit (Roche, 11175041910) was used. Tissues were incubated for 3 h in blocking solution then, overnight at 4 °C, with 100 µl per slice of 1/2000 v/v anti-digoxigenin-AP-conjugated antibody 750 U/ml. According to the kit guidelines, slices were washed in MABT baths before being developed overnight at 4 °C in NBT/BCIP. Finally, slices were mounted in Mowiol mounting medium and then dried for 48 h at 4 °C, before being observed using a Nikon Eclipse 80i microscope equipped with NIS-Elements D 3.0 software (Nikon Instruments).

2.7. Immunohistochemistry (IHC) and immunocytofluorescence (ICF)

Tissues embedded in paraffin were cut into 5 µm slices which were deparaffined in roti-histol baths (Roth, 6640.2), rehydrated using successive ethanol dilutions (100 %, 96 %, 75 % and 50 %) and washed in PBS before antigen unmasking (2 × 90s, micro-waves 600W followed by a 1 h cooling period). Endogenous peroxidase activities were blocked using 3 % hydrogen peroxide in PBS and non-specific labeling was blocked using 0.1 % Triton in PBS with 1 % BSA. Slices were incubated overnight at 4 °C with the primary antibody (rabbit polyclonal anti-human TSHR antibody, 1:2000, Abcam, ab202960 or rabbit IgG polyclonal-isotype control, 1:2000, Abcam, ab37415) diluted in Antibody Diluent (Abcam, ab64211), then washed in PBS before a 2h incubation at room temperature with the secondary antibody (Goat anti-rabbit H&L IgG, HRP polymer, 1:1, Abcam, ab214880). After washing, the DAB Substrate Kit (3.3′-diaminobenzidine, Abcam, ab64238) was applied until staining (2–60 min). Then, the slices were counterstained with Groat's hematoxylin, rinsed with tap water, dehydrated in successive baths of ethanol (50 %, 75 %, 96 % and 100 %) and roti-histol (Roth, 6640.2), and mounted into roti®histokit media (Roth, 6638.1).

ICF was performed to verify the expression of recombinant proteins and the antibody specificity used in IHC analyses. HEKT293T cells transfected with pTarget-*Sctshr* plasmid were washed twice using PBS with 1 % BSA, collected and fixed with 4 % PFA for 15 min before attachment to polysine slides (Epredia). The cells were permeabilized with 0.1 % Triton in PBS buffer with 1 % BSA for 5 min then incubated overnight at 4 °C with the rabbit polyclonal anti-human TSHR antibody (1:500, Abcam, ab202960) or with the rabbit IgG polyclonal-isotype control (1:500, Abcam, ab37415). The cells were then washed and incubated for 2 h at room temperature with the Alexa Fluor™ 488 goat anti-rabbit IgG (H&L) (1:250, Invitrogen, A-11008) secondary antibody. After washes, the cells were mounted in Prolong™ Gold Antifade Mountant with 40,6-diamidino-2-phenylindole (DAPI) (P36935). Pictures were taken using the Eclipse 80i microscope (Nikon) with the same exposure time for each antibody, independently of the sample tested.

2.8. Western blot

Frozen tissues from testicular zones A, B, C, and D, proximal and distal segments of the epididymis, ovary, and thyroid gland were crushed in liquid nitrogen, extracted with 2.5 vol of ice-cold lysis buffer (6M urea, 2M thiourea, 40 mM Tris-base, 2 % CHAPS, 1 mM EDTA, 0.5 mM DTT, 1 mM AEBSF, and 10 µM E64 protease inhibitors), then sonicated and kept for 1 h on ice before being centrifuged at 15 000 g for 30 min at 4 °C. Supernatants were then centrifuged at 105 000 g for 1 h at 4 °C. Protein concentration of resulting supernatants was determined using the bicinchoninic acid (BCA) protein assay (Sigma-Aldrich, Merck,

France). Extracted proteins (500 ng) were resolved on 10 % gel electrophoresis before blotting on a PVDF membrane (Cytiva Amersham, RPN303F). After a 1-h blocking step in PBS with 10 % non-fat dried milk, the membranes were probed overnight at 4 °C with one of the following primary antibodies: mouse monoclonal anti-human actin antibody (1:1000, Sigma, A3853); rabbit polyclonal anti-human TSHR antibody (1:500, Abcam, ab202960); rabbit IgG polyclonal-isotype control (1:500, Abcam, ab37415). After a 2-h incubation with the corresponding secondary antibody, the goat anti-rabbit IgG (H&L) HRP polymer antibody (1:1, Abcam, ab214880) or the goat anti-mouse IgG (H&L) HRP polymer antibody (1:1, Abcam, ab214879), and washes, the DAB Substrate Kit (3.3′-Diaminobenzidine, Abcam, ab64238) was applied until staining (2–60 min).

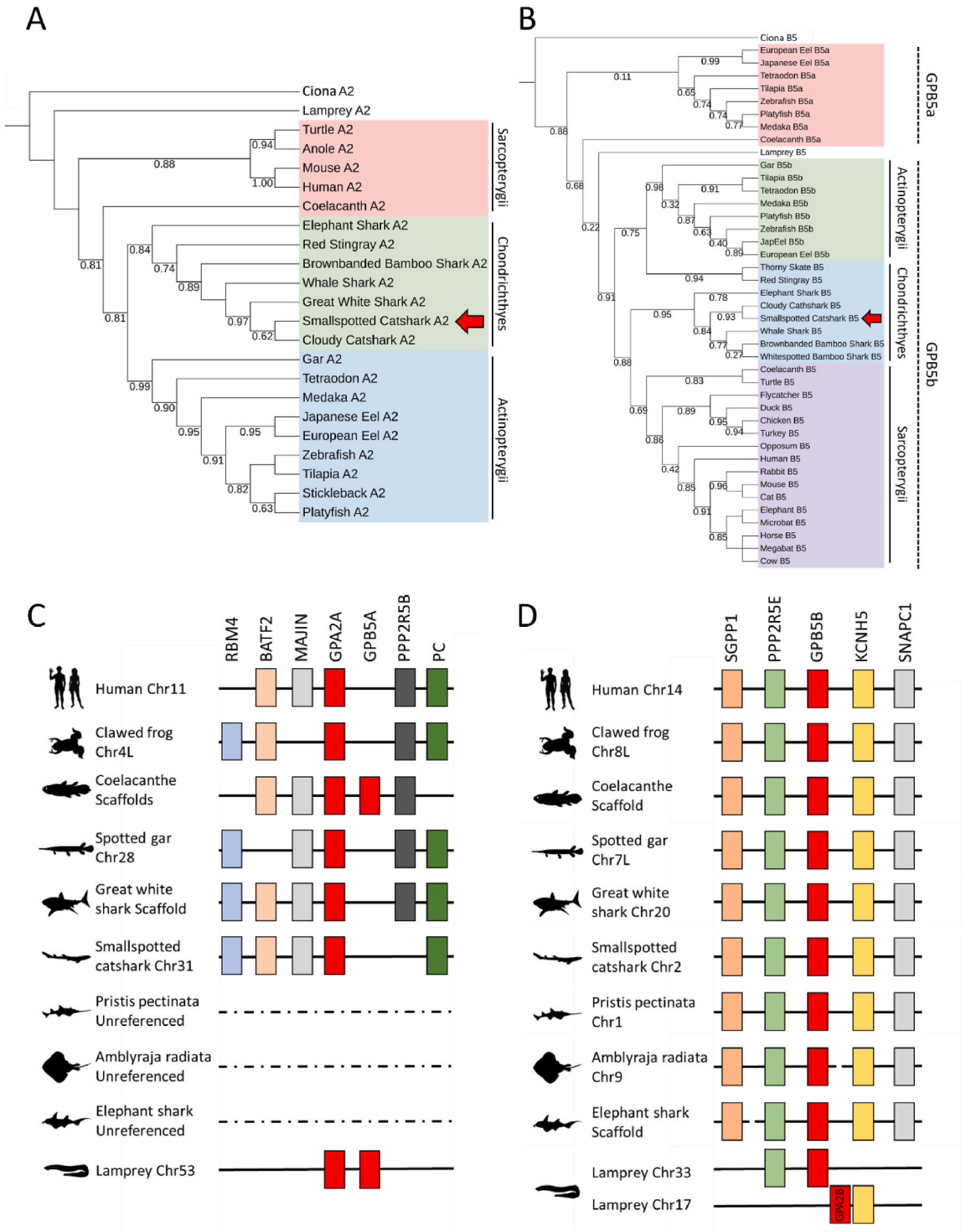

Fig. 1. *In silico* characterization of elasmobranchian GPA2 and GPB5. Molecular phylogeny of GPA2 (A) and GPB5 (B). *Scyliorhinus canicula* proteins are highlighted by red arrows. Support values shown are bootstraps for 1000 replicates. Sequences used are listed (Supplementary Data, Excel). Synteny of the genomic region flanking *gpa2* and *gpb5a* genes (C) and *gpb5b* gene (D) in vertebrate species. The chromosome numbers are indicated. The coelacanth genomic regions were used as reference. Animal illustrations are used with permission from http://phylopic.org.

3. Results

3.1. GPA2a, GPB5b, TSHβ2 and TSHR sequences identified in elasmobranch genomes

Sequence searches were carried out based on sequences identified in *C. milii* and predicted sequences available in the NCBI database for *S. canicula*. Of the nine elasmobranch genomes analyzed, one TSHβ gene was identified for each, and *gpa2* and/or *gpb5* genes were identified in only 5 genomes and not in those of the batoid *A. radiata*, and of the sharks *C. carcharias*, *C. plagiosum*, and *P. pectinata*. The subsequent phylogenetic analysis including a maximum of GPH subunits and TSHR sequences validated their annotations. The molecular phylogeny of the GPA2s (Fig. 1A) showed that the chondrichthyan sequences segregated together and that the holocephalan GPA2 was rooted with the selachian sequences. Molecular phylogeny of the GPB5 subunits (Fig. 1B) showed that the chondrichthyan sequences were grouped with GPB5b sequences and not with GPB5a sequences, and the holocephalan GPB5 rooted with the shark sequences while batoidea sequences were grouped with actinopterygii sequences. Synteny analyses of *gpa2*-and *gpb5*-related gene regions confirmed the presence of *gpa2*, but not of *gpb5a*, in the genomes of *C. carcharias* and of *S. canicula* as well as the high conservation of the *gpb5b* gene region in the analyzed chondrichthyes (Fig. 1C and D). In addition, the *gpa2a-gpb5a* tandem and the *gpa2b*- and the *gpb5b*-related gene regions were conserved in the *P. marinus* genome. Genes coding protein phosphatase 2 regulatory subunit (PPP2R5) isoforms were located on the genomic fragments close to *gpa2* and *gpb5* genes. Molecular phylogeny of the TSHR orthologs showed that the chondrichthyan sequences were grouped in agreement with the phylogeny, and the holocephalan TSHR rooted the batoidea and selachii groups (Fig. 2A). The molecular phylogeny of TSHβs showed that elasmobranch orthologs segregated with the *C. milii* TSHβ2 while the *C. milii* TSHβ1 rooted with the sarcopterygian sequences, which suggests the retention of the *tshβ2* gene and the loss of the *tshβ1* gene in elasmobranchs (Fig. 2B). Synteny analyses of *tshβ1*-and *tshβ2*-related genes regions in gnathostomes confirmed the absence of the *tshβ1* gene in the genomes of *A. radiata*, *C. carcharias* and *S. canicula* (Fig. 2C), while *tshβ2* gene was localized in a highly conserved region, also found in *C. milii*

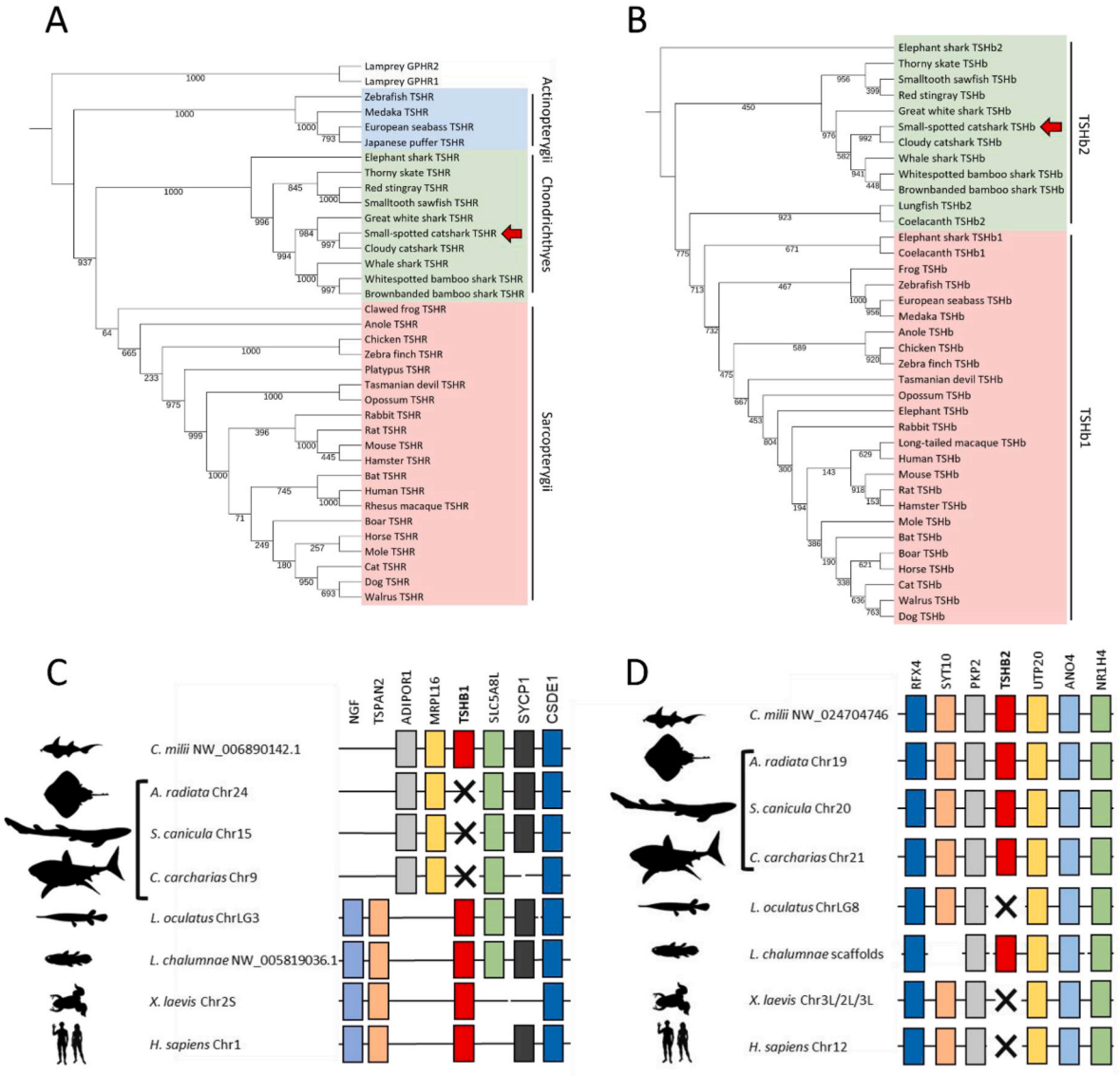

Fig. 2. *In silico* characterization of elasmobranchian TSHR and TSHβ2. Molecular phylogeny of TSHR (A) and TSHβ (TSHβ1 and TSHβ2) (B). *S. canicula* proteins are highlighted by red arrows. Support values shown are bootstraps for 1000 replicates. Sequences used are listed (Supplementary Data, Excel). Synteny of the genomic region flanking *tshb1* (C) and *tshb2* genes (D) in representative species of vertebrate groups. The chromosome numbers are indicated. The *C. milii* genomic regions were used as reference. Animal illustrations are used with permission from http://phylopic.org.

and *L. chalumanae* (Fig. 2B).

3.2. Globally conserved structures of GPA2, GPB5, TSHβ2 and TSHR, excepted a shorter "seat-belt" domain of GPB5 and a structure divergence of the hinge and P10 loops for TSHR

The primary structures of elasmobranchs GPA2, GPB5, TSHβ2 and TSHRs were analyzed based on knowledge of human orthologs. Alignment of the Chondrichthyan GPA2 and GPB5 sequences has shown 10 conserved cysteines (C), 2 putative N-glycosylation sites, a "seat" region conserved in all Gpb5 and Gpa2 of elasmobranchs, except for *H. akajei* sequence with a histidine (H) instead of a tyrosine (Y), and the "seat-belt" region of GPB5 comprising only two conserved C (Supplementary Fig. S2). Concerning alignment of the chondrichthyan TSHβ2 subunit sequences, it has shown 12 conserved C residues involved in disulfide bonds, including the four characteristic C of the "seat-belt" and 1 N-glycosylation site (Supplementary Fig. S3). The "seat" region was conserved in elasmobranchs and diverged from the holocephalan sequence with a phenylalanine (F) instead of a tyrosine (Y). Multiple alignments of the protein sequences of TSHR (Supplementary Fig. S4) have shown, in their large extracellular domains, 35 well-conserved leucine (L) residues, 2 N-glycosylation sites, and a conserved putatively sulfated tyrosine residue. The putative limit between the solenoid and the "hinge" region was predicted. The transmembrane region of the chondrichthyan TSHRs was composed of 7 putative α-helical transmembrane domains (TM), 2 conserved cysteines, one APPL1, one ERW, one Ubiquitin interaction, and PKC2 binding domain, and one BXXBB putative motif. The C-terminal region exhibits a putative $F(X)_6LL$ motif, an S/T cluster, a second BXXBB putative motif, and a L-palmitoyl site.

The predicted models were constructed using the Q96T91.1.A template and the resulting pieces of information (Supplementary Table S2) reflected the fit between them. The closer GMQE and QMEANDisCo Global scores are to 1, the closer the predicted model is to the template. The TSHβ2 predicted models showed overall sequence identities relative to the Q96T91.1.A template of *H. sapiens* of 57.92 % and 59.41 % for *C. milii* and *S. canicula*, respectively. Despite these identities, the structural discrepancies were low since the GMQE and QMEANDisCo Global scores were only 0.06 to 0.08 lower for TSHβ2 predicted models of *C. milii* and *S. canicula* compared to the human control model (Supplementary Table S3). Scores obtained for TSHR models were relatively high with global sequence identities of 75.99 % and 73.20 %, GMQE and QMEANDisCo Global scores 0.02 to 0.06 lower than those of the human control template for *C. milii* and *S. canicula*, respectively. Compared to the human template, discrepancies in predicted models were slightly more important for GPA2 than for GPB5. For *C. milii* and *S. canicula* GPA2 models, respectively, global sequence identities were 58.68 % and 63,39 %; GMQE scores were 0.41 and 0.42 lower and QMEANDisCo Global scores were 0.23 and 0.20 lower than the human template scores. For *C. milii* and *S. canicula* GPB5 models, respectively, global sequence identities were 79.44 % and 72,31 %, GMQE scores were 0.24 and 0.30 lower and QMEANDisCo Global scores were 0.15 and 0.21 lower than the human template scores. The predicted models of TSHβ, GPA2, and GPB5 obtained for *S. canicula* and *C. milii* proteins were superposable, including the cystine knot structures, and highlighted the shorter "seat-belt" domain of GPB5, with a very low mean RMSD ranging from 0.03 to 1.77 Å (Fig. 3A–F). In contrast, the TSHR solenoid superposition had a very low mean RMSD of 0.07 Å, which includes the hinge helix with the Serine scS280 (Fig. 3G and H), suggesting a conservation of the hinge helix and the solenoid structures among all these species. However, the mean RMSD of 19.32 Å associated with the hinge loop and the P10 loop appeared much higher, suggesting their divergence. Furthermore, the putative sulfotyrosine site (scY_{385}) was highly conserved (Fig. 3G). This analysis showed structure conservations of GPA2, GPB5, and TSHβ, including the cystine knot, the absence of the "seat-belt" in GPB5 orthologs, and conservation of the TSHR ectodomains, including hinge helix and sulfotyrosine site, while structure divergence was associated to hinge and P10 loops.

3.3. The single-chain recombinant ScGPB5-ScGPA2 stimulates ScFSHR, ScLHR and ScTSHR in in vitro assays

HEK293T cells coexpressing *Sc*FSHR/$G\alpha_{16}$ subunit, *Sc*LHR/$G\alpha_{16}$ or *Sc*TSHR/$G\alpha_{16}$ were stimulated by serial concentrations, assayed by nanoLC-ESI-MS/MS, of *Sc*GPA2, *Sc*GPB5, or the single-chain recombinant *Sc*GPB5-*Sc*GPA2 or *Sc*TSHβ2-*Sc*CGA (Fig. 4). Dose-response analyses based on Ca^{2+} detection have shown that *Sc*GPA2, *Sc*GPB5 and *Sc*GPB5-*Sc*GPA2 were able to activate *Sc*FSHR-expressing cells over a picomolar to nanomolar concentration range, with higher potency for *Sc*GPB5-*Sc*GPA2 and *Sc*GPB5 than for *Sc*GPA2 (Fig. 4A–Table 1). For *Sc*LHR-expressing cells, dose-response profiles were similar to those obtained with *Sc*FSHR-expressing cells, with potencies in the same order of magnitude (Fig. 4B–Table 1). For *Sc*TSHR-expressing cells, the potency of *Sc*GPB5-*Sc*GPA2 was slightly higher than that of *Sc*TSHβ2-*Sc*CGA, which was used as a control (Fig. 4C–Table 1).

3.4. High relative expression of tshr and gpb5 mRNAs during spermiogenesis in S. canicula

The expression profiles of transcripts were analyzed in 35 different tissues including the male and female genital tract, brain and thyroid (Fig. 5). As expected, the highest level of *tshr* mRNA was observed in the thyroid of males and females, but high levels were also observed in testis, with a 10-fold increase from the zone A to zone D, the proximal segment of the epididymis, and the lymphomyeloid Leydig organ of males (Fig. 5A and B). In females, high levels of *tshr* mRNA were observed in the brain and genital tract, particularly in the oviduct and nidamental gland (Fig. 5A). A broad tissue expression profile of the *gpa2* mRNA was observed, in both males and females, with high levels in the different brain regions, particularly the cerebellum and the male forebrain, and in the thyroid (Fig. 5A). High levels were also observed in Leydig organ (Fig. 5A). In the male genital tract, the highest *gpa2* mRNA level was observed in seminal ampullae, high levels were observed in proximal and distal segments of the epididymis, and testis in which, *gpa2* mRNA levels were three-fold higher in zone A, containing the germinative area and cysts with spermatogonia, than in the subsequent stages of spermatogenesis (Fig. 5A–C). In the female genital tract, higher *gpa2* mRNA levels were observed in the oviduct and nidamental gland than in the ovary and uterus (Fig. 5A). In contrast, the tissue expression profile for *gpb5* appeared more restricted than for *gpa2* with the highest levels observed in testis (Fig. 5A), with a 160-fold increase from the zone A to the zone D (Fig. 5D). During spermatogenesis, the two increases of *gpb5* and *tshr* mRNA levels were significantly correlated by a Spearman correlation test (P-value = 0.020). Outside the testis, *gpb5* appeared moderately expressed in the brain but not at all in the male tract, contrasting with the *gpa2* profile (Fig. 5A–D). In females, low levels of *gpb5* mRNA were observed in the ovary (Fig. 5A–D). For *tshβ2*, expression analysis showed the highest mRNA levels in males' and females' middle-brain/pituitary, lower levels in the male forebrain, cerebellum, and myelencephalon, the lowest mRNA levels in male epididymis, in female forebrain and myelencephalon, and ovary, and no expression in testis, seminal ampullae and female cerebellum (Fig. 5E).

3.5. Expression of gpa2 in germ cells and of tshr/TSHR and gpb5 in epithelial cells, including Sertoli cells and epididymis, in the male genital tract of S. canicula

In situ analyses were performed in genital tract tissues using real-time PCR results to identify the cell types expressing the transcripts and proteins of interest. In order to further validate the antibodies used, immunocytofluorescence was performed on HEK293T cells expressing *Sc*TSHR (Supplementary Fig. S5) as well as by Western blot analysis (Supplementary Fig. S6). The results showed that the rabbit polyclonal

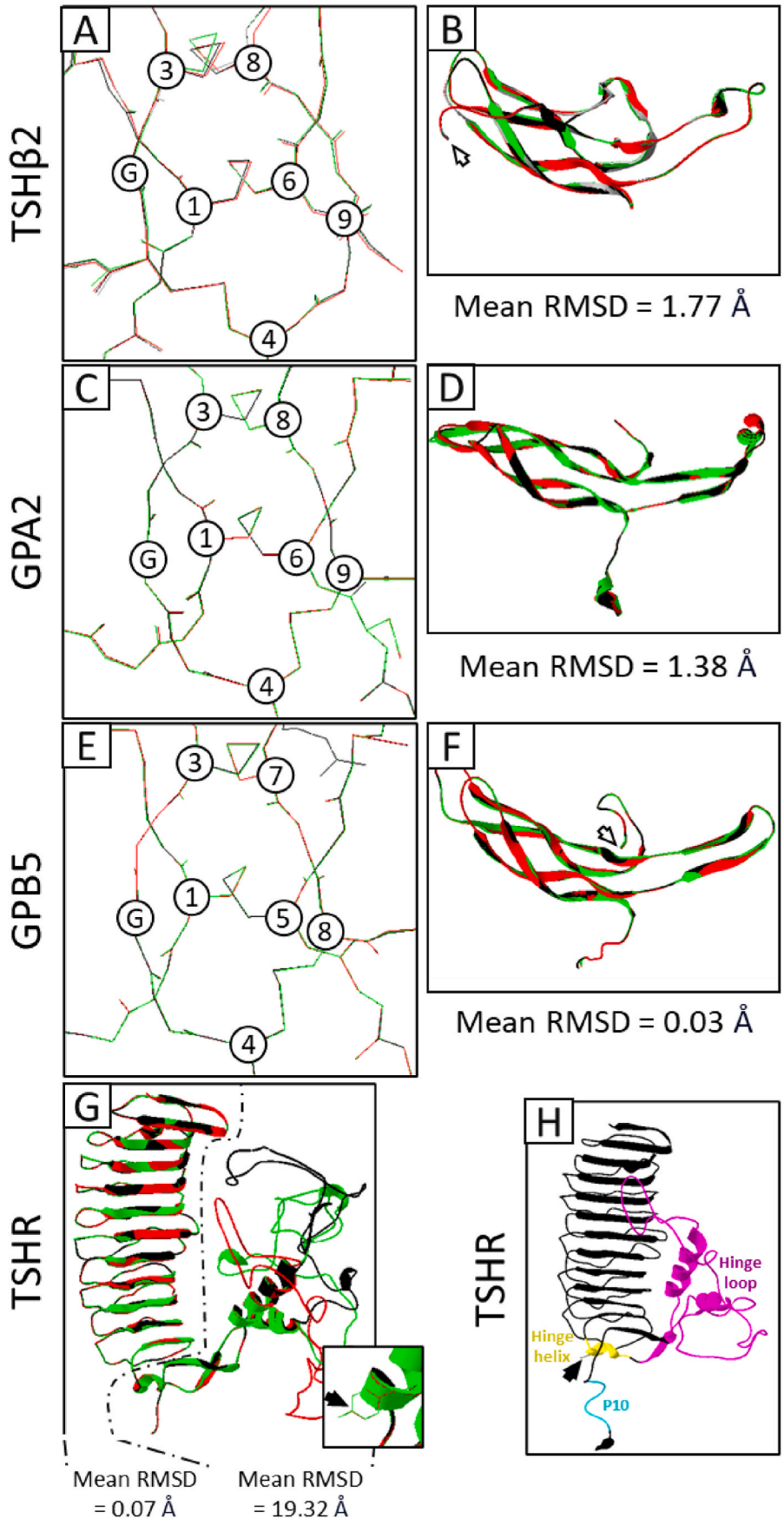

(caption on next page)

Fig. 3. *In silico* analysis of the 3D structures of *S. canicula, C. milii* and *H. sapiens* TSHβ, GPA2, GPB5 and TSHR. (A), (C), (E) Superpositions of the 8-aa-ring cystine-knot structure and (G) of the TSHR ectodomains, (H) TSHR model of *S. canicula* highlighting the hinge helix in yellow with the S280 (black arrowhead), the hinge loop in purple and the P10 loop in blue of the hinge region, (B, D, F) of the hormone subunits with RMSD means. The *H. sapiens* TSHβ model (used as a template) and *C. milii* TSHβ1, *C. milii* TSHβ2 and *S. canicula* TSHβ2 predicted models are illustrated in green, grey, black and red, respectively. White arrowhead, C-terminal extremity with or without the "seat-belt" region; Black arrowhead, putative sulfotyrosine.

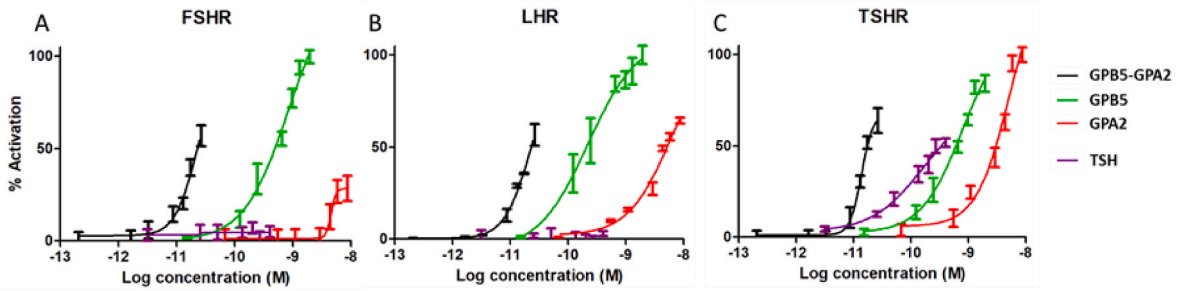

Fig. 4. Dose-responses of cells expressing *Sc*FSHR, *Sc*LHR or *Sc*TSHR induced by recombinant *Sc*GPA2, *Sc*GPB5 or single-chain *Sc*GPB5-*Sc*GPA2. (A–C) Dose-dependent calcium responses of HEK293T cells coexpressing *Sc*GPHR/*hs*Gα_{16} treated with serial dilutions of conditioned medium from HEK293T transfected with corresponding pTarget *gpa2*, *gpb5* or *gpb5-gpa2* plasmids and whose recombinant protein concentrations were assayed by nanoLC-ESI-MS/MS. *Sc*TSH was used as a control. All experiments were performed in duplicate and the most representative was selected for ligand absolute quantification using high-resolution nanoLC-ESI-MS/MS. Data are shown as relative (%) to the highest value (100 % activation) for a given ligand and represent the mean of an experiment (n = 3).

Table 1
Efficiency (EC_{50}) and efficacy (Emax) of *Sc*GPA2, *Sc*GPB5, *Sc*GPB5-*Sc*GPA2 or *Sc*TSH on *Sc*FSHR, *Sc*LHR and *Sc*TSHR.

	Efficiency (EC_{50}) nM				Efficacy (Emax) %			
	ScGPA2	*ScGPB5*	*ScGPB5-ScGPA2*	*ScTSH*	*ScGPA2*	*ScGPB5*	*ScGPB5-ScGPA2*	*ScTSH*
*Sc*FSHR	4.512 ± 0.226	0.837 ± 0.042	0.021 ± 0.004	N/A	27.64 ± 1.21	100.00 ± 4.29	48.51 ± 12.21	N/A
*Sc*LHR	5.846 ± 0.292	0.221 ± 0.011	0.025 ± 0.003	N/A	59.96 ± 6.26	100.00 ± 6.19	46.15 ± 14.82	N/A
*Sc*TSHR	5.164 ± 0.258	0.790 ± 0.040	0.014 ± 0.001	0.169 ± 0.008	100.00 ± 3.36	83.33 ± 1.44	58.00 ± 2.52	51.80 ± 4.59

N/A: not applicable.

TSHR antibody exhibited a specific signal in the cytoplasm and cell membrane of TSHR-expressing cells compared with the control corresponding to cells transfected with the empty plasmid (Supplementary Figure S5A1, A2). However, the rabbit IgG polyclonal-isotype control exhibited a low unspecific signal in the cytoplasm and cell membrane of both *Sc*TSHR-expressing cells and cells transfected with the empty plasmid (Supplementary Figure S5B1, B2). On Western blot, two bands of about 90 and 50 kDa were detected with the anti-human TSHR rabbit polyclonal antibody (Supplementary Fig. S6A) in extracts of all testicular zones (A, B, C, and D), as well as of proximal and distal epididymis, ovary and thyroid. The band of 90 kDa could correspond to the full-length receptor, based on its theoretical molecular weight of 85 kDa, and the band of 50 kDa to the extracellular domain of the receptor, based on its theoretical molecular weight of 46 kDa after cleavage at position 406 of the protein sequence (Supplementary Fig. S4). The use of the rabbit IgG, polyclonal-isotype control revealed protein bands around 90 and 75 kDa but none corresponding to TSHR (Supplementary Fig. S6B). The immunohistochemistry of TSHR evidenced specific staining in the cytoplasmic extensions of differentiated Sertoli cells, localized between germ cells, in cysts with spermatogonia, with spermatocytes, with round spermatids, and in the basal cytoplasm, surrounding the nucleus of Sertoli cells in cysts with elongated spermatids (Fig. 6A1-D1). Immunolabelling of the cyst lumen or interstitial tissue was unspecific according to the results obtained with the rabbit IgG polyclonal-isotype control (Fig. 6A2-D2). In agreement with the immunodetection of TSHR, the ISH results showed the localization of *tshr* mRNA transcripts in the cytoplasm of differentiated Sertoli cells (Fig. 6A3-D3). The ISH of *gpa2* transcripts exhibited staining associated with the cytoplasm of spermatogonia, spermatocytes, rounds spermatids and associated to the head of elongated spermatids (Fig. 7A1-D1). In contrast, ISH of *gpb5* showed an initial significant staining in the cytoplasm of Sertoli cells only in cysts containing round spermatids and elongated spermatids (Fig. 7C3-D3), in agreement with RT-PCR results (Fig. 5D). In the last stage of spermatogenesis, the ISH signal was clearly localized in the basal cytoplasm of the Sertoli cells, surrounding nuclei, and in the thin cytoplasmic projections around the head of spermatids (Fig. 7D3).

In situ analyses were completed by a study of the lymphomyeloid epigonal tissue associated with the testis, the testicular collecting tubules, the proximal and distal epididymis, the lymphomyeloid Leydig's gland and the thyroid. Strong staining was observed in the epigonal tissue for both TSHR/*tshr* (Fig. 6E1-E4) and *gpb5* (Fig. 7E3), apparently associated with granulocytes. In the next part of the male genital tract, epithelial cells of the collecting tubules expressed TSHR/tshr (Fig. 8A2-A5) and *gpb5* (Fig. 8E4), epithelial cells of the proximal (Fig. 8B1-B5) and distal (Fig. 8C1-C5) epididymis expressed TSHR/*tshr* (Fig. 8B2, B4, C2, C4) and *gpa2* (Fig. 8F2, G2), and the epithelial cells of Leydig gland's expressed TSHR/*tshr* (Fig. 8D2, D4) and *gpa2* (Fig. 8H2). In the thyroid, TSHR/*tshr*-associated staining (Fig. 9A2-A5) and *gpa2*-associated staining (Fig. 9C2-C3) were observed in the follicular epithelium. The absence of signal for *gpb5* mRNA in segments of epididymis (Fig. 8F4, G4) and in the thyroid gland (Fig. 9C4) was in agreement with the RT-PCR results (Fig. 5A–D). Furthermore, *in situ* expression analyses were extended to ovarian follicles containing differentiated granulosa and theca cells, used as a control rather than for in-depth study since literature reported expressions of GPA2, GPB5 and TSHR in mammalian ovarian follicles. Here, theca cells and oocyte expressed TSHR/*tshr*, *gpa2* and *gpb5* while granulosa cells expressed only *gpb5* (Fig. 9B2-B5, D2-D5).

4. Discussion

Recently, the genome of several chondrichthyes allowed significant

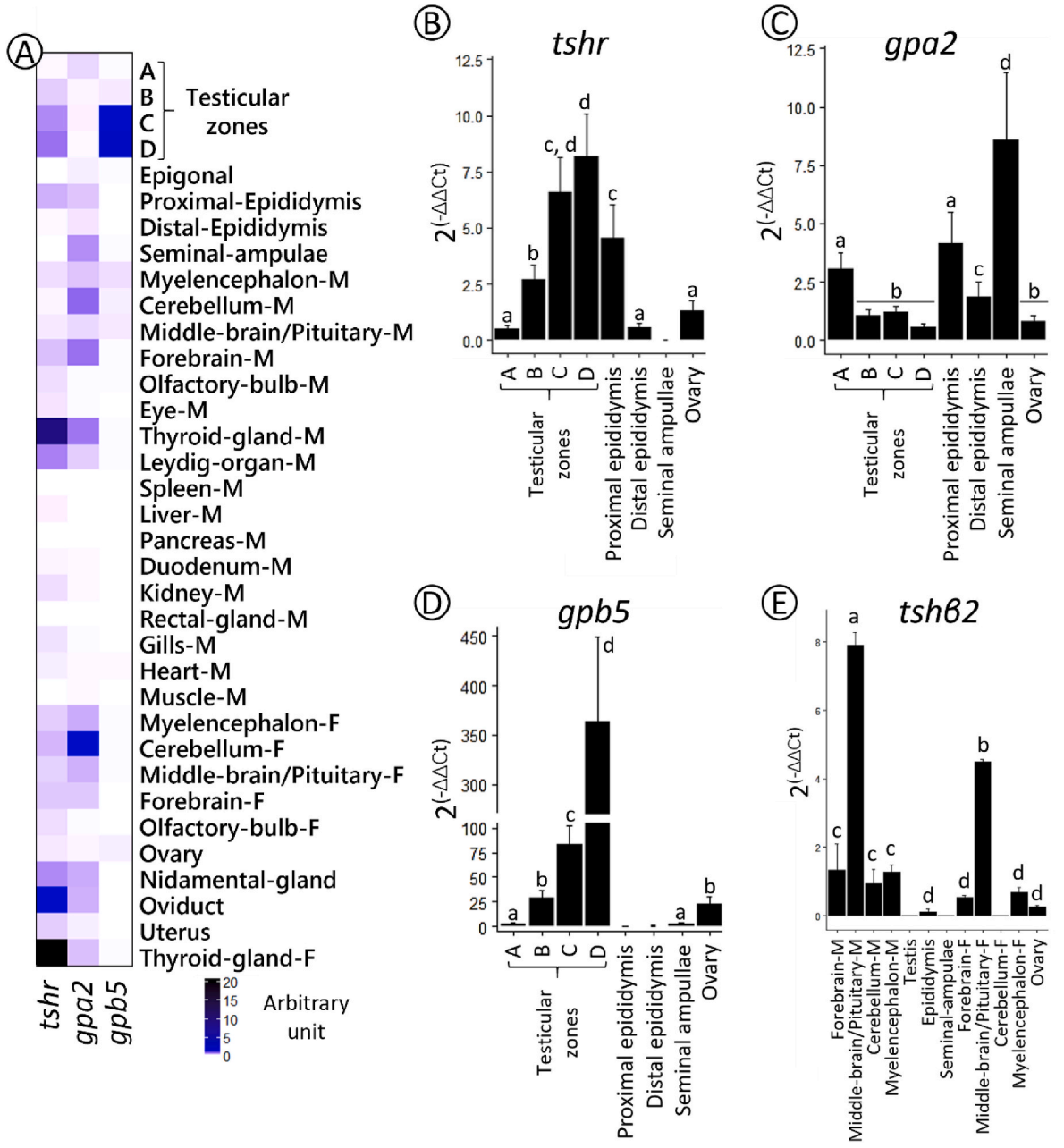

Fig. 5. Relative expression profiles of *tshr*, *gpa2*, *gpb5* and *tshβ* transcripts in *S. canicula* tissues with a focus on the male genital tract. Messenger RNA levels were assayed by real-time PCR. (A) Warm map representation of relative gene expression in 35 different tissues. Relative gene expression of *gpa2* (B), *gpb5* (C) and *tshr* (D) along the male genital tract and in the ovary. E. Relative gene expression of *tshβ2* in four different parts of the brain and along the male genital tract. Statistical analysis was performed using the Mann-Whitney *U* test with a P-value <0.05 between each statistical groups a, b, c and d. A, B, C and D: testicular zones from six animals in triplicates (N = 6; n = 18); other tissues: from three animals in triplicates (N = 3; n = 9). The tissues from females correspond to females caught in September (non-breeding period) whose ovaries contained a few early vitellogenic follicles. M, Male; F, Female.

advances in phylogeny of genes regulating reproduction in vertebrates, including those of the glycoprotein hormones (GpHs) and their receptors (GpHRs) such as in the holocephalan *C. milii* (Buechi and Bridgham, 2017) and the elasmobranchs *R. typus*, *C. punctatum* and *S. torazame* (Arimura et al., 2024; Hara et al., 2018). One of our study's aims was to complete the characterization of GpHs and GpHRs in Elasmobranchs by analysis of more, now available, genomes. Our results allowed the identification of *gpa2* and/or *gpb5* genes in four additional species, including the red stingray *H. akajei*, the thorny skate *A. radiata*, the great white shark *C. carcharias,* and the small-spotted catshark *S. canicula.* Furthermore, these results confirmed that the *tshβ2* gene, but not the *tshβ1* gene, was maintained in elasmobranch genomes, underlining the divergence with the holocephalan *C. milii* genome where both genes are present (Buechi and Bridgham, 2017; Maugars et al., 2014).

Outstanding predicted structures of GPHs were found conserved in the elasmobranch TSHβs, GPA2s, and GPB5s. Most importantly, the cysteine residues, all involved in disulfide bonds, were found at homologous positions thus allowing 1/the formation of the cystine-knots in all GPH subunits as well as in GPA2 and GPB5 and 2/the "seatbelt" fastening by the C3-C12 bridge ("buckle") in all GPHβ subunits but not in GPB5s lacking these two cysteine residues. The absence of the seatbelt in GPB5 raised the question of the stability of the GPA2/GPB5 heterodimer in the peripheral circulation (Alvarez et al., 2009). The putative N-glycosylation sites and the characteristic "seat" region

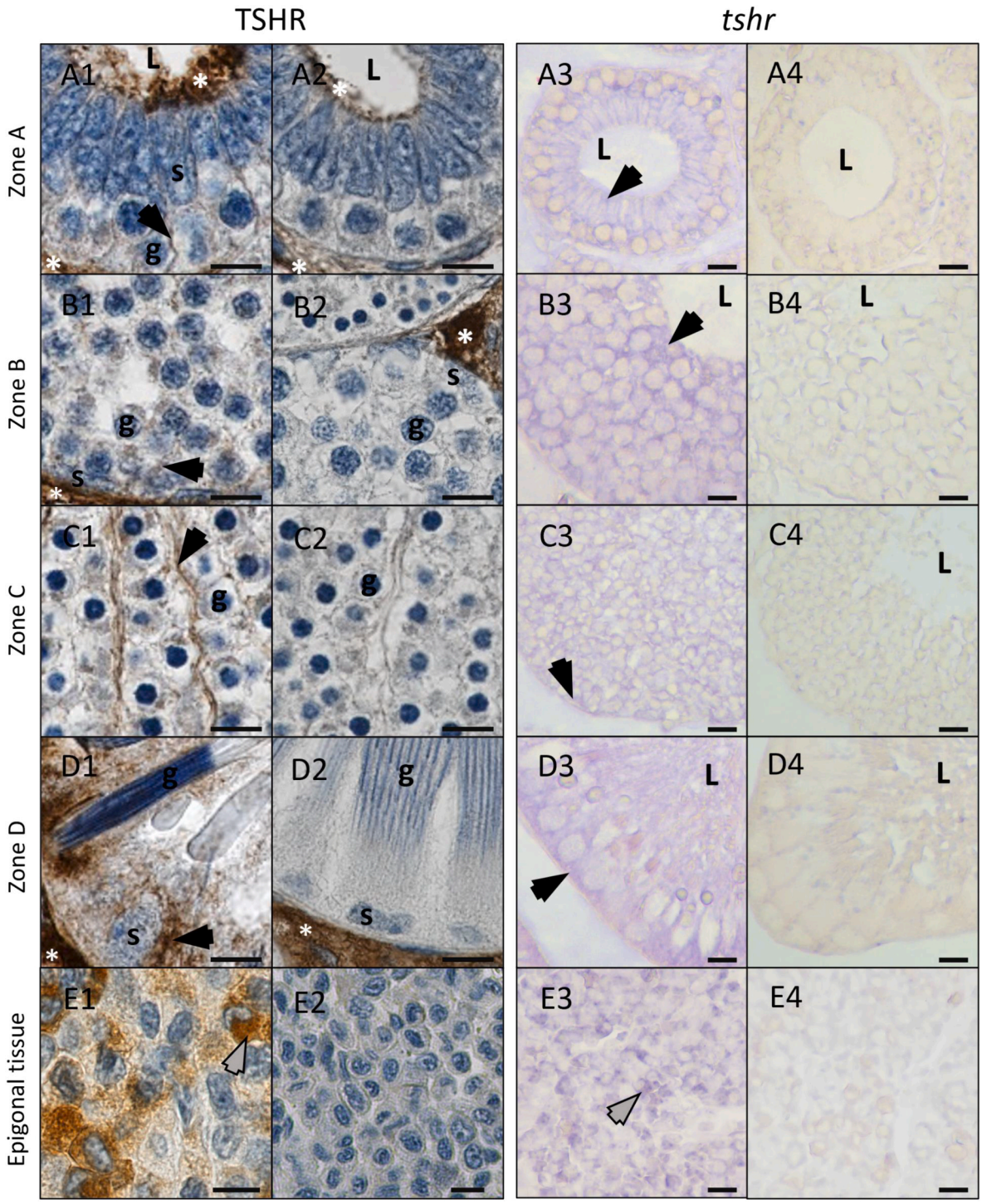

Fig. 6. Immunohistochemistry of TSHR and *in situ* hybridization of *tshr* mRNA in *S. canicula* testicular sections. The testicular zones A, B, C and D correspond to formed cysts with spermatogonia (A1-A4), to cysts with primary spermatocytes (B1-B4), cysts with young spermatids (C1-C4) and cysts with late spermatids (D1-D4), respectively. The lymphomyeloid epigonal tissue is illustrated (E1-E4). Immunohistochemistry was performed with the rabbit polyclonal anti-human TSHR antibody (1:2000, Abcam, ab202960) (A1-E1) and control performed with the rabbit IgG polyclonal isotype control (human) antibody (1:2000, Abcam, ab37415) (A2-E2). The secondary antibody used was the goat HRP polymer anti-rabbit IgG H&L (1:1, Abcam, ab214880). In *situ* hybridization was performed with antisense riboprobes targeting *Sctshr* mRNA (A3-E3) and control with sense riboprobes of *Sctshr* mRNA (A4-E4). For immunostaining and revelation, the DIG-Nucleic Acid Detection Kit was used. Black arrowhead, staining associated with Sertoli cells (A1-D1, A3-D3); grey arrowhead, staining associated with granulocytes (E1, E3); g: germ cell nuclei; L: lumen; s: sertolian nuclei; asterix: unspecific staining. Scale bars: 10 μm.

involved in α- and β-subunits interaction are also conserved.

Compared with the GTHR of *C. milii* (Buechi and Bridgham, 2017) and *H. sapiens* (Ulloa-Aguirre et al., 2018), the primary structures of the TSHR identified in elasmobranchs were highly conserved with the leucine-rich solenoid, hinge, N-glycosylation and sulfation sites in their ectodomains. In the human LHCGR, the hinge region includes a hinge helix (residues 276–282), a hinge loop (residues 284–340) and a P10 loop (residues 350–359), and hydrophobic mutations of the hinge helix,

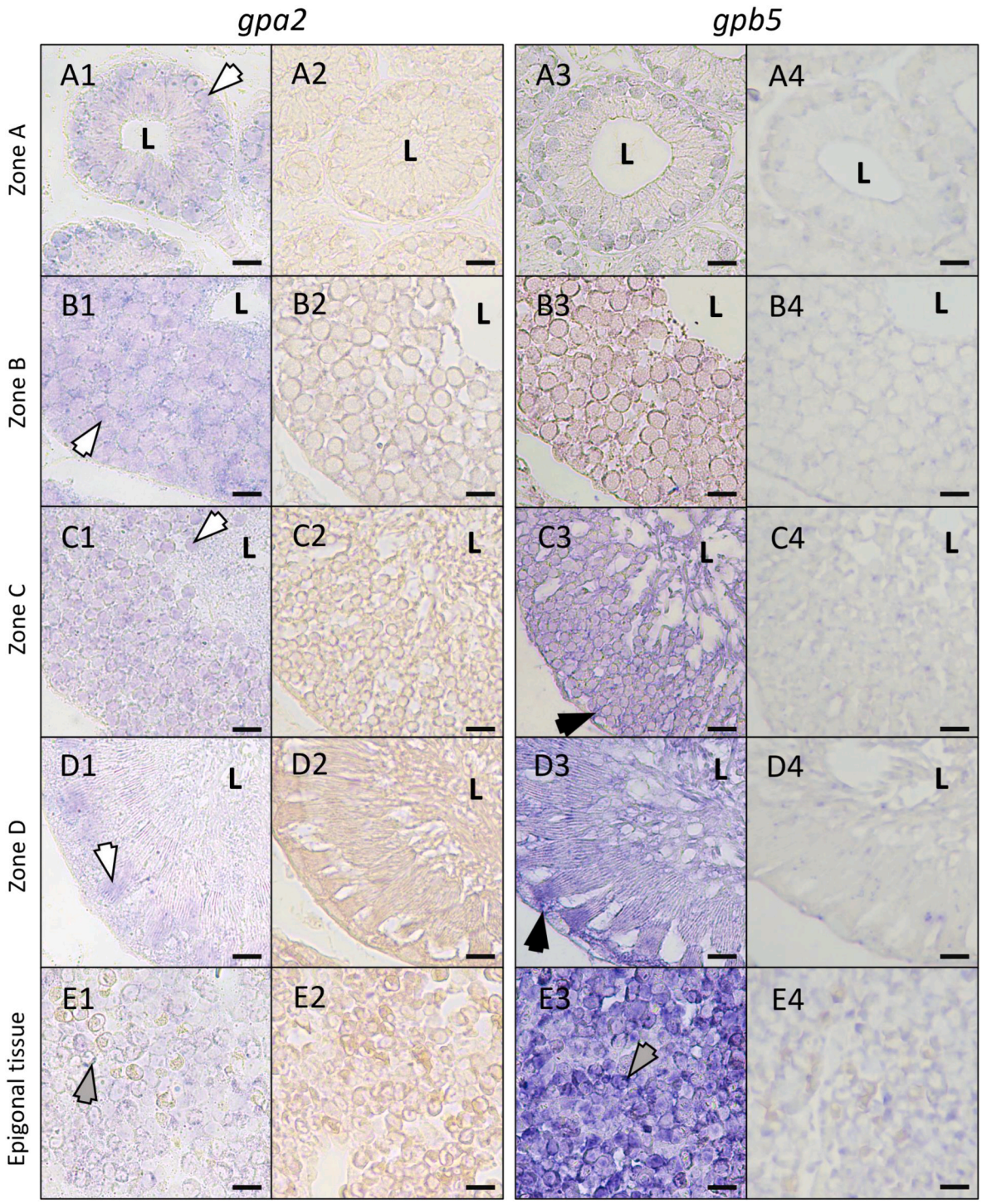

Fig. 7. I*n situ* hybridization of *gpa2* and *gpb5* mRNAs in *S. canicula* testicular sections. The testicular zones A, B, C and D correspond to formed cysts with spermatogonia (A1-A4), to cysts with primary spermatocytes (B1-B4), cysts with young spermatids (C1-C4) and cysts with late spermatids (D1-D4), respectively. *In situ* hybridization was performed with antisense riboprobes targeting *Scgpa2* mRNA (A1-E1) or *Scgphb5* mRNA (A3-E3) and control with sense riboprobes of *Scgpa2* mRNA (A2-E2) or of *Scgphb5* mRNA (A4-E4). The DIG-Nucleic Acid Detection Kit was used for revelation. White arrowhead, staining associated with the germ cells (A1-D1); black arrowhead, staining associated with Sertoli cells (C3-D3); grey arrowhead, staining associated with granulocytes (E1, E3); g: germ cell nuclei; L: lumen; s: sertolian nuclei. Scale bars: 10 μm.

notably of the serine residue at position 277, alters the receptor activation property, as also noted for TSHR (He et al., 2022; Jaeschke et al., 2011; Mueller et al., 2009). In comparison, the TSHR sequence of *S. canicula* shows a highly conserved serine residue (*Sc*TSHR S280). At the same time, a significant conformational difference was observed for the hinge loop, possibly causing a conformational change in the P10 loop as observed in our model. However, the sequence and the 3D conformation of the potentially sulfated tyrosine (Y_{385}) implied in a high-affinity ligand-receptor interaction were conserved. These results suggest that during evolution, the hinge loop has diverged the most, although the consequence for ligand/receptor interaction specificity remains to be defined. Primary structures of the seven transmembrane

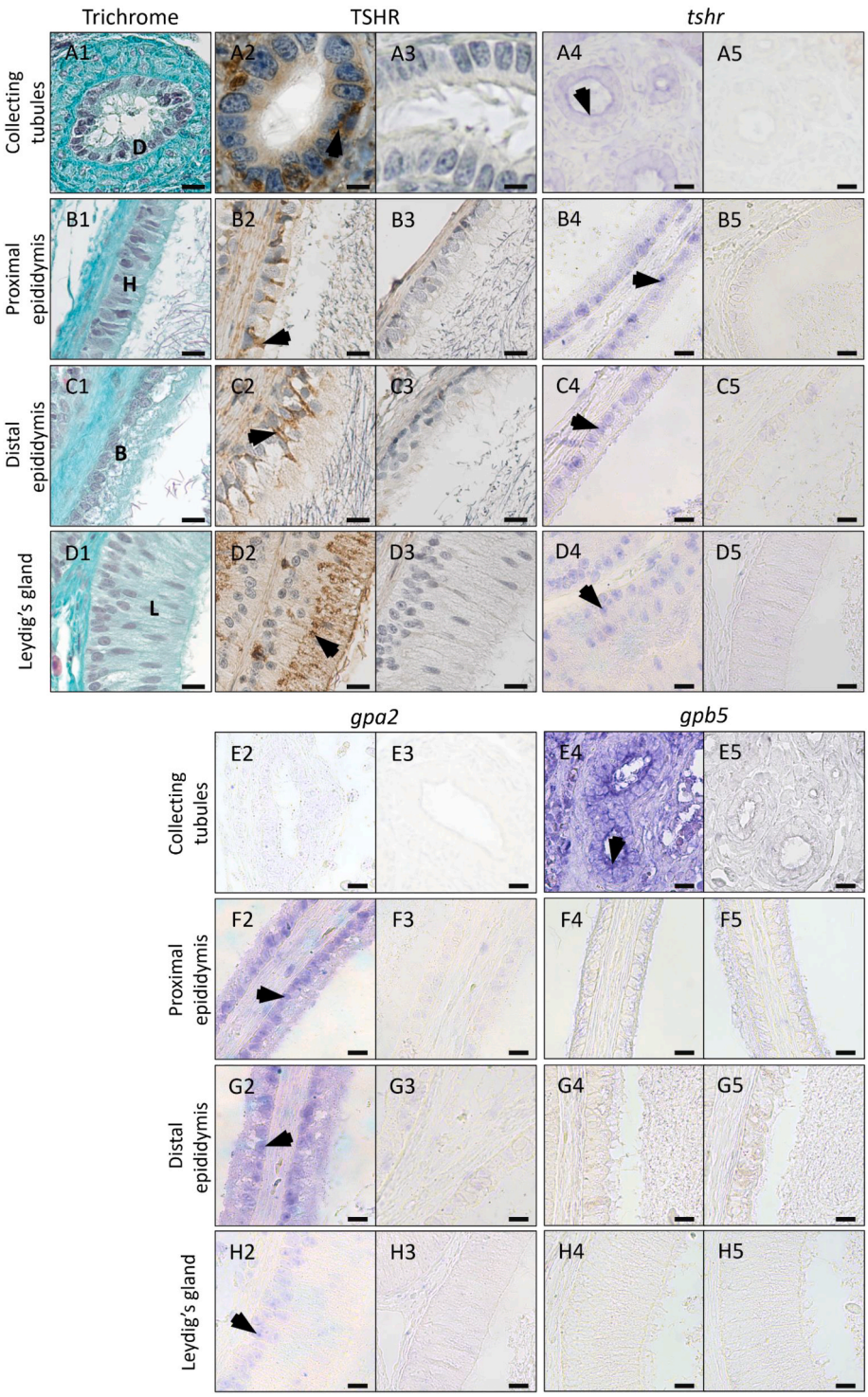

Fig. 8. Immunohistochemistry of TSHR and *in situ* hybridization, t*shr*, *gpa2* and *gpb5* mRNAs in the male genital tract of *S. canicula*. Histology of testis collecting tubules (A1), proximal epididymis (B1), distal epididymis (C1), and the Leydig's gland (D1). Immunohistochemistry was performed with the rabbit polyclonal anti-human TSHR antibody (1:2000, Abcam, ab202960) (A2-D2) and control performed with the rabbit IgG polyclonal isotype control (human) antibody (1:2000, Abcam, ab37415) (A3-D3). *In situ* hybridization was performed with antisense riboprobes targeting Sc*tshr* mRNA (A4-D4), Sc*gpa2* mRNA (E2-H2) or Sc*gpb5* mRNA (E4-H4), and control was performed with sense riboprobes of *Sctshr* mRNA (A5-D5), *Scgpa2* mRNA (E3-H3) or of *Scgphb5* mRNA (E5-H5). In the male genital tract, expressions of TSHR/*tshr* and *gpb5* were observed in the epithelial cells of collecting tubules (A2, A4; F2), of TSHR/*tshr* and *gpa2* in epithelial cells of proximal epididymis (B2, B4; F2), distal epididymis (C2, C4; G2), and Leydig's gland (D2, D4; H2) (black arrowhead). B: epithelium of the distal epididymis; D: epithelium of collecting tubules; H: epithelium of the proximal epididymis; L: Leydig's gland. Scale bars: 10 μm.

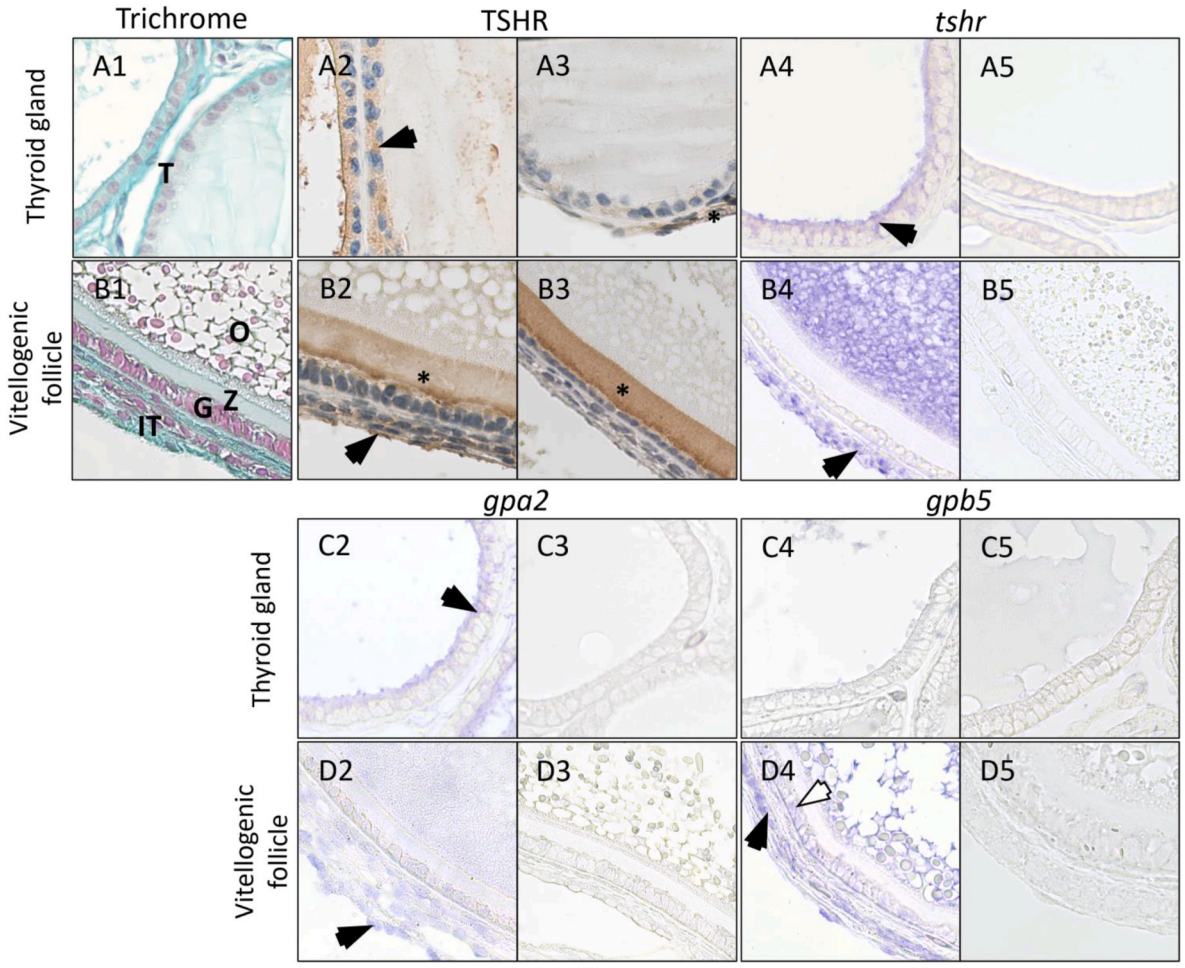

Fig. 9. Immunohistochemistry of TSHR and *in situ* hybridization of t*shr*, *gpa2* and *gpb5* mRNAs in the male thyroid gland and in the vitellogenic follicle of *S. canicula*. Histology of thyroid gland (A1) and vitellogenic follicle (B1). Immunohistochemistry was performed with the rabbit polyclonal anti-human TSHR antibody (1:2000, Abcam, ab202960) (A2, B2) and control performed with the rabbit IgG polyclonal isotype control (human) antibody (1:2000, Abcam, ab37415) (A3, B3). *In situ* hybridization was performed with the antisense riboprobes targeting S*ctshr* mRNA (A4, B4), *Scgpa2* mRNA (C2, D2) or *Scgpb5* mRNA (C4, D4). Expressions of TSHR/*tshr* and *gpa2* were observed in epithelial cells of thyroid follicle (A2, A4; C2) (black arrowhead). In the vitellogenic follicle, expressions of TSHR/*tshr*, *gpa2* and *gpb5* were observed in the theca cells (black arrowhead) and *gpb5* was additionally observed in the granulosa cells (white arrowhead) (B2-B5; D2-D5). Asterix: unspecific staining; G: granulosa layer; IT: inner theca layer; T: epithelium of the thyroid gland follicle; O: ooplasm; Z: zona pellucida. Scale bars: 10 μm.

α-helixes were also conserved with APPL1, ERW, BXXBB, ubiquitin interacting, and PKC2 binding domains in intracellular loops 1, 2, and 3, respectively.

In the present study, ligand-receptor interaction analyses using HEK293T cells transiently transfected with *Scfshr*, *Sclhr* or *Sctshr* together with the promiscuous *hs*Gα_{16} showed that the recombinant *Sc*TSHβ2-*Sc*CGA, expressed as a single-stranded protein, could activate only *Sc*TSHR, in agreement with the previous report concerning *C. milii* (Buechi and Bridgham, 2017). Thus, for the first time in an elasmobranch, it has been shown that *Sc*GPB5-*Sc*GPA2 can activate *Sc*TSHR, as previously observed in *R. norvegicus* and *H. sapiens* (Nagasaki et al., 2006; Nakabayashi et al., 2002). However, the EC_{50} of single-chain *Sc*GPB5-*Sc*GPA2 on *Sc*TSHR is ten times lower than those found for human and rat thyrostimulins, but the efficiency of *Sc*TSH on *Sc*TSHR was similar to the bovine TSH on bTSHR (Nagasaki et al., 2006; Okajima et al., 2008).

Most interestingly, the recombinant single strand *Sc*GPB5-*Sc*GPA2 also activated *Sc*FSHR and *Sc*LHR in addition to *Sc*TSHR. This surprising result fits well with the previously proposed "negative specificity" model (Combarnous, 1992; Combarnous and Hengé, 1981). Indeed, in this model, the seatbelt sequence in the β-subunits wraps around their α-counterpart to stabilize the heterodimer formation but also determines specificity by inhibiting the binding (hence "negative specificity") of each heterodimer to the other GPHRs. Since *Sc*GPB5-*Sc*GPA2 remains dimeric thanks to the β-α sequences' fusion but lacks seatbelt sequence, there is no inhibition towards any of the GPHRs, thus leading to binding and activation of all of them.

This result suggests a more ancestral function or a specificity of the receptors not yet established, as it was described in the lamprey *P. marinus* where GPB5-GPA2 could activate both GPHRI and GPHRII (Hausken et al., 2018). In addition, recombinant *Sc*GPB5 alone could also activate *Sc*FSHR, *Sc*LHR, and *Sc*TSHR but with a tenfold lower efficiency than the single-chain *Sc*GPB5-*Sc*GPA2. The recombinant *Sc*GPA2 could also activate the three *Sc*GPHRs, but probably only at a supraphysiological concentration. Observed efficacies also suggest agonist and partial agonist activities of *Sc*GPB5 and *Sc*GPA2-*Sc*GPB5, respectively, on *Sc*FSHR and *Sc*LHR. Our results are, however, in contradiction with those obtained in the holocephalan *C. milii*, where heterodimeric *Cm*GPA2 and *Cm*GPB5 subunits or single-chain *Cm*GPB5-*Cm*GPA2 failed to activate *Cm*TSHR (Buechi and Bridgham, 2017). This lack of activation could result from the use of a receptor with a truncated hinge loop (XP_007904236.1), whereas a full-length receptor (XP_042194080.1) was predicted later in 2021 by automated computational analysis. In our study, we were unable to determine if *Sc*GPA2 or *Sc*GPB5 were active as monomer or homodimer, which is a matter of debate in different species, along with the issue of the

endocrine or paracrine role of the GPA2/GPB5 heterodimer. In mammals, the fact that thyrostimulin has been claimed to activate *h*TSHR as a non-covalent heterodimer whereas systemic blood GPA2 and GPB5 concentrations were much below the dimerization Kd. This suggests a paracrine role for the non-covalent GPA2/GPB5 heterodimer but also raises the issue of the potential endocrine role(s) of separated GPA2 and GPB5 units (Alvarez et al., 2009; Sun et al., 2010). In the basal chordate *B. japonicum*, each GPA2 or GPB5 monomer could bind the amphioxus GPHR (named TSHR by the authors and also referred to as LGR1) without activating it, only the recombinant single-chain GPB5-GPA2 was able to do so, suggesting a local role of monomers as antagonists of GPHR (Wang et al., 2018). In the ascidian *S. clava*, GPA2 and GPB5 are secreted by distinct secretory pathways and could activate, as recombinant single-chain GPB5-GPA2, HEK293T cells expressing GPHR (Yang et al., 2023). However, the separate GPA2 and GPB5 have not been tested. In the mosquito *A. aegypti*, it has also been suggested that GPA2 and GPB5 may form homodimers. Still, only the single-chain GPB5-GPA2 modulates the activity of the mosquito GPHR (LGR1) (Rocco and Paluzzi, 2020). In the lamprey, GPA2 heterodimerizes with GPB5 and the recombinant fusion protein GPB5-GPA2 can activate the lamprey GpH receptors I and II; however, GPA2 and GPB5 have not been tested separately (Hausken et al., 2018). Overall, heterodimerization of GPA2 and GPB5 seems necessary, and it has been suggested that they may have evolved from an ancestral homodimer consisting of two GPA2s in basal metazoans, based on the study of the crystal structure of the heterodimer GPA2/GPB5 of *C. elegans* secreted by transfected HEK293S cells (Gong et al., 2023). The dose-responses observed in our study when *Sc*GPA2 or *Sc*GPB5 are expressed alone would therefore not be incompatible with this evolutionary history from homodimers.

In numerous species, GPB5 exhibits a much more restricted tissue expression than GPA2. Nevertheless, coexpression of GPA2 and GPB5 was observed in a few locations but mainly outside the brain and pituitary or pituitary-like organs; for example, in the gonads in ecdysozoans (Rocco et al., 2017; Rocco and Paluzzi, 2020; Vandersmissen et al., 2014), basal chordates (Wang et al., 2018; Yang et al., 2023); lamprey (Hausken et al., 2018) and mammals (Li et al., 2004; Nagasaki et al., 2006; Nakabayashi et al., 2002; Okada et al., 2006). Our results on the tissue expression profiles of GPA2 and GPB5 observed in *S. canicula* agree with these previous studies since their coexpression was observed in the gonads, notably in the testes. In *S. canicula*, although we did not precisely study its brain localization by *in situ* analyses, our results show the highest expression of *tshβ2* in the midbrain, including the hypothalamus and pituitary, of both males and females, which was in agreement with an expression in the ventral lobe of the pituitary of sharks (Hara et al., 2018). *Tshr*, *gpa2,* and *gpb5* genes were also coexpressed in different parts, suggesting paracrine regulation of the central nervous system involving TSH/TSHR and/or (GPA2/GPB5)/TSHR signaling, as in the regulation of food intake in rats (Burgos et al., 2016) or seasonality in fishes, birds and mammals (Irachi et al., 2021; Yoshimura, 2010). Our results also show that *tshr* and TSHR were expressed in the epithelial cells of thyroid follicles, as expected. Still, extrathyroidal expressions of the TSHR, outside the thyroid and brain, were observed in the testis and epididymis, the lymphomyeloid Leydig organ, and the oviduct and nidamental gland. In testis, *tshr* mRNA and TSHR protein levels increased from early to late stages of spermatogenesis with localization in somatic precursors and differentiated Sertoli cells. These results are in agreement with TSHR expression observed in Sertoli cells of *R. norvegicus* (Fadlalla et al., 2017), but not *H. sapiens* (Li et al., 2022), and in the testis of some teleost as in the Walking catfish, *Clarias batrachus* (Bhat et al., 2017), Channel catfish, *Ictalurus punctatus* (Goto-Kazeto et al., 2009), striped bass, *Morone saxatilis* (Kumar et al., 2000), and European sea bass, *Dicentrarchus labrax* (Rocha et al., 2007). In *D. labrax*, it has been proposed involvement of TSHR signaling in gonadal development, spermiogenesis, and spermiation (Rocha et al., 2007). In the absence of *tshβ2* expression in the testis of *S. canicula* and based on functional assays, *Sc*GPA2/*Sc*GPB5 can be expected to exert a paracrine role in the regulation of spermatogenesis by activating testicular TSHR, without ruling out an endocrine action of circulating TSH. This is also reinforced by the correlation observed between *gpb5* and *tshr* mRNA levels during spermatogenesis. Although it is difficult to determine precise expression colocalization in the absence of the use of a fluorescence approach, *in situ* analysis showed *gpa2* expression in germ cells while *gpb5* and *tshr* were expressed in the Sertoli cells, suggesting paracrine and/or autocrine regulations. Further studies are needed to determine how these regulations are coupled to those through testicular FSHR and LHR expressions recently studied in the catshark (Jeanne et al., 2024). Interestingly, the downregulation of the putative GPA2/GPB5 receptor (LGR1) in the mosquito *A. aegypti* impacted spermatozoa differentiation (Rocco et al., 2019), underlining the ancestral involvement of GPA2/GPB5 in spermiogenesis. However, the deletion of either GPB5 or GPA2 in mice did not produce an overt phenotype (Okada et al., 2006), raising the question of the biological role of GPA2 and GPB5 during spermatogenesis in organisms with differentiated gonadotropic hormones. Nevertheless, the double KO of both *gpa2* and *gpb5* genes has not been performed so it cannot be excluded that GPA2 and GPB5 exert similar functions and can rescue each other.

In the male genital tract of *S. canicula*, significant *gpa2,* and *tshr* mRNA levels were observed in the proximal segment of the epididymis. *In situ* analyses localized *tshr* transcripts and protein in the epithelium of testicular collecting tubules, co-expressed with *gpb5* but not *gpa2*. Then, TSHR was localized in the epithelium of proximal and distal segments of the epididymis and epithelial cells of Leydig's gland. In the epididymis, we show for the first time that *tshr* is co-expressed with *gpb5*. In mammals, spermatozoa acquire their motility and fertilizing properties during their epididymal transit (Dacheux and Dacheux, 2014; Sullivan et al., 2005) may be related to their internal fertilization mode (Gervasi and Visconti, 2017). In elasmobranchs, which also have internal fertilization, epididymis has been poorly studied despite its similarity to mammals. However, studies in sharks and batoids have shown that the epididymis participates in luminal fluid modifications and that spermatozoa acquired their motility during their transit in the distal epididymal segment of the epididymis (Dzyuba et al., 2019; Jones et al., 1984). The Leydig gland, which is adjacent to the epididymis and secretes part of the seminal fluid into the deferent duct, seems to be involved in spermatozoa aggregation, occurring into seminal ampullae, to form spermatozeugmata or spermatophores, according to species (Jones et al., 2005). Another specificity of elasmobranchs, is the presence of lymphomyeloid tissues forming the gonad-associated epigonal tissue and the gut-associated Leydig organ (different from the Leydig gland). Our results show that the epigonal tissue expressed *tshr* and *gpb5* and the Leydig organ expressed *tshr* and *gpa2*. The biological significance of these co-expressions has to be clarified but, interestingly, previous studies have suggested a cross-talk between the epigonal tissue and the gonads in elasmobranchs (Lutton and Callard, 2007; Piferrer and Callard, 1995).

Expression analyses of *S. canicula* females showed high levels of *tshr* and *gpa2* transcripts in the oviduct and nidamental gland and lower levels in the ovary, as also observed for *gpb5* transcripts. Although the tissues were only taken from females outside their reproductive period and corresponded to ovaries with few vitellogenic follicles, *in situ* analyses showed an expression of TSHR/*tshr* in theca layers and oocyte, of *gpa2* in granulosa cells and of *gpb5* in theca and granulosa cells. Although our analysis remains limited, these follicular expressions are in agreement with a paracrine GPA2/GPB5/TSHR signaling as characterized in the *R. norvegicus* ovary (Sun et al., 2010).

5. Conclusion

In conclusion, our study shows that, *in vivo*, *gpb5* is highly expressed in *S. canicula* testis. *In vitro,* the recombinant single-chain *Sc*GPB5-*Sc*GPA2 dimer, as well as *Sc*GPB5 alone, activate the three *S. canicula*

GPHRs (*Sc*FSHR, *Sc*LHR, and *Sc*TSHR) in a comparable potency range, suggesting their implications in the paracrine regulation of spermatogenesis, an implication that remains to be clarified. Chondrichthyes, as the most ancient clade with differentiated GPHs and GPHRs, could exhibit a transitional endocrine system between the pleiotropic GPA2/GPB5/GPHR signaling found in the cyclostomes and early gnathostomes and the specific GtHs/GtHRs signaling in all other gnathostomes (actinopterygians and sarcopterygians).

CRediT authorship contribution statement

Fabian Jeanne: Writing – review & editing, Writing – original draft, Resources, Methodology, Investigation, Formal analysis, Data curation, Conceptualization. **Stanislas Pilet:** Resources, Methodology, Investigation, Formal analysis. **Yves Combarnous:** Writing – review & editing, Investigation, Formal analysis. **Benoît Bernay:** Writing – review & editing, Resources, Methodology, Investigation, Formal analysis, Data curation, Conceptualization. **Sylvie Dufour:** Writing – review & editing, Investigation, Formal analysis. **Pascal Favrel:** Writing – review & editing, Resources, Methodology, Investigation, Formal analysis, Conceptualization. **Pascal Sourdaine:** Writing – review & editing, Resources, Project administration, Methodology, Investigation, Funding acquisition, Formal analysis, Data curation, Conceptualization.

Declaration of competing interest

Authors declare no conflict of interest.

Acknowledgments

The authors are grateful to Didier Leroy from the CGFS (Channel Ground Fish Survey) campaign (IFREMER in the East Manche in September 2022) for providing the catsharks and to Frédérique Guyon of the “Centre de Recherches en Environnement Côtier” (Luc sur Mer, France) for the care given to the animals. Authors thank Danièle Klett for helpful dicussions. The following are thanked for funding: University of Caen Normandy (F.J.’s PhD grant), European Regional Development Fund (Operational Programme ERDF/ESF 2014–2020) under the project “Manche 2021 – Plateformes d’exploitation de ressources marines”, Région Normandie under the project “Emergent−CauSy.

Appendix. ASupplementary data

Supplementary data to this article can be found online at https://doi.org/10.1016/j.mce.2025.112553.

Data availability

Data will be made available on request.

References

Alvarez, E., Cahoreau, C., Combarnous, Y., 2009. Comparative structure analyses of cystine knot-containing molecules with eight aminoacyl ring including glycoprotein hormones (GPH) alpha and beta subunits and GPH-related A2 (GPA2) and B5 (GPB5) molecules. Reprod. Biol. Endocrinol. 7, 90. https://doi.org/10.1186/1477-7827-7-90.

Arimura, S., Wong, M.K.S., Inoue, R., Kawano, M., Shimoyama, K., Fujimori, C., Tokunaga, K., Takagi, W., Hyodo, S., 2024. Functional characterization of follicle-stimulating hormone and luteinizing hormone receptors in cloudy catshark, Scyliorhinus torazame. Gen. Comp. Endocrinol. 354, 114542. https://doi.org/10.1016/j.ygcen.2024.114542.

Atwood, B.K., Lopez, J., Wager-Miller, J., Mackie, K., Straiker, A., 2011. Expression of G protein-coupled receptors and related proteins in HEK293, AtT20, BV2, and N18 cell lines as revealed by microarray analysis. BMC Genom. 12, 14. https://doi.org/10.1186/1471-2164-12-14.

Bassett, J.H.D., Van Der Spek, A., Logan, J.G., Gogakos, A., Bagchi-Chakraborty, J., Murphy, E., Van Zeijl, C., Down, J., Croucher, P.I., Boyde, A., Boelen, A., Williams, G.R., 2015. Thyrostimulin regulates osteoblastic bone formation during early skeletal development. Endocrinology 156, 3098–3113. https://doi.org/10.1210/en.2014-1943.

Bhat, I.A., Rather, MohdA., Saha, R., Ganie, P.A., Sharma, R., 2017. Identification and expression analysis of thyroid stimulating hormone receptor (TSHR) in fish gonads following LHRH treatment. Proc. Natl. Acad. Sci. India B Biol. Sci. 87, 719–726. https://doi.org/10.1007/s40011-015-0640-8.

Buechi, H.B., Bridgham, J.T., 2017. Evolution of specificity in cartilaginous fish glycoprotein hormones and receptors. Gen. Comp. Endocrinol. 246, 309–320. https://doi.org/10.1016/j.ygcen.2017.01.007.

Burgos, J.R., Iresjö, B.-M., Wärnåker, S., Smedh, U., 2016. Presence of TSH receptors in discrete areas of the hypothalamus and caudal brainstem with relevance for feeding controls—support for functional significance. Brain Res. J. 1642, 278–286. https://doi.org/10.1016/j.brainres.2016.04.007.

Cahoreau, C., Klett, D., Combarnous, Y., 2015. Structure-function relationships of glycoprotein hormones and their subunits’ ancestors. Front. Endocrinol. 6, 26. https://doi.org/10.3389/fendo.2015.00026.

Cho, S., Rogers, K.W., Fay, D.S., 2007. The C. elegans glycopeptide hormone receptor ortholog, FSHR-1, regulates germline differentiation and survival. Curr. Biol. 17, 203–212. https://doi.org/10.1016/j.cub.2006.12.027.

Combarnous, Y., 1992. Molecular basis of the specificity of binding of glycoprotein hormones to their receptors. Endocr. Rev. 13, 670. https://doi.org/10.1210/edrv-13-4-670, 670.

Combarnous, Y., Hengé, M.H., 1981. Equine follicle-stimulating hormone. Purification, acid dissociation, and binding to equine testicular tissue. JBC 256, 9567–9572. https://doi.org/10.1016/S0021-9258(19)68799-5.

Cuevas, M.E., Callard, G., 1992. In vitro steroid secretion by staged spermatocysts (sertoli/germ cell units) of dogfish (Squalus acanthias) testis. Gen. Comp. Endocrinol. 88, 151–165. https://doi.org/10.1016/0016-6480(92)90204-W.

Dacheux, J.-L., Dacheux, F., 2014. New insights into epididymal function in relation to sperm maturation. Reproduction 147, R27–R42. https://doi.org/10.1530/REP-13-0420.

Dong, J., Xin, M., Liu, H., Zhang, M., Pang, Q., Chen, L., Zhao, B., 2013. Identification, expression of a glycoprotein hormone receptor homolog in the amphioxus Branchiostoma belcheri with implications for origin of vertebrate GpHRs. Gen. Comp. Endocrinol. 184, 35–41. https://doi.org/10.1016/j.ygcen.2012.08.006.

Dos Santos, S., Bardet, C., Bertrand, S., Escriva, H., Habert, D., Querat, B., 2009. Distinct expression patterns of glycoprotein hormone-α2 and -β5 in a basal chordate suggest independent developmental functions. Endocrinology 150, 3815–3822. https://doi.org/10.1210/en.2008-1743.

Dufour, S., Quérat, B., Tostivint, H., Pasqualini, C., Vaudry, H., Rousseau, K., 2020. Origin and evolution of the neuroendocrine control of reproduction in vertebrates, with special focus on genome and gene duplications. Physiol. Rev. 100, 869–943. https://doi.org/10.1152/physrev.00009.2019.

Dzyuba, V., Ninhaus-Silveira, A., Kahanec, M., Veríssimo-Silveira, R., 2019. Sperm motility in ocellate river stingrays: evidence for post-testicular sperm maturation and capacitation in chondrichthyes. J Zool 307, 9–16. https://doi.org/10.1111/jzo.12610.

Fadlalla, M.B., Wei, Q., Fedail, J.S., Mehfooz, A., Mao, D., Shi, F., 2017. Effects of hyper- and hypothyroidism on the development and proliferation of testicular cells in prepubertal rats. Anim. Sci. J. 88, 1943–1954. https://doi.org/10.1111/asj.12883.

Gautron, J., 1978. Effet du calcium et de la stimulation sur les terminaisons nerveuses des fonctions nerf-électroplaque de la Torpille. Biol. Cell. 31, 31–44. https://doi.org/10.1007/BF00495387.

Gervasi, M.G., Visconti, P.E., 2017. Molecular changes and signaling events occurring in spermatozoa during epididymal maturation. Andrology 5, 204–218. https://doi.org/10.1111/andr.12320.

Giraldo, C., Le Roy, D., Martin-Baillet, V., 2022. CGFS2022 cruise, RV Thalassa. https://doi.org/10.17600/18001842.

Gong, Z., Wang, W., El Omari, K., Lebedev, A.A., Clarke, O.B., Hendrickson, W.A., 2023. Crystal structure of LGR ligand α2/β5 from Caenorhabditis elegans with implications for the evolution of glycoprotein hormones. Proc. Natl. Acad. Sci. USA 120, e2218630120. https://doi.org/10.1107/S205979832300102X.

Goto-Kazeto, R., Kazeto, Y., Trant, J.M., 2009. Molecular cloning, characterization and expression of thyroid-stimulating hormone receptor in channel catfish. Gen. Comp. Endocrinol. 161, 313–319. https://doi.org/10.1016/j.ygcen.2009.01.009.

Hara, Y., Yamaguchi, K., Onimaru, K., Kadota, M., Koyanagi, M., Keeley, S.D., Tatsumi, K., Tanaka, K., Motone, F., Kageyama, Y., Nozu, R., Adachi, N., Nishimura, O., Nakagawa, R., Tanegashima, C., Kiyatake, I., Matsumoto, R., Murakumo, K., Nishida, K., Terakita, A., Kuratani, S., Sato, K., Hyodo, S., Kuraku, S., 2018. Shark genomes provide insights into elasmobranch evolution and the origin of vertebrates. Nat. Ecol. Evol. 2, 1761–1771. https://doi.org/10.1038/s41559-018-0673-5.

Hausken, K.N., Tizon, B., Shpilman, M., Barton, S., Decatur, W., Plachetzki, D., Kavanaugh, S., Ul-Hasan, S., Levavi-Sivan, B., Sower, S.A., 2018. Cloning and characterization of a second lamprey pituitary glycoprotein hormone, thyrostimulin (GpA2/GpB5). Gen. Comp. Endocrinol. 264, 16–27. https://doi.org/10.1016/j.ygcen.2018.04.010.

He, X., Duan, J., Ji, Y., Zhao, L., Jiang, H., Jiang, Y., Eric Xu, H., Cheng, X., 2022. Hinge region mediates signal transmission of luteinizing hormone and chorionic gonadotropin receptor. CSBJ 20, 6503–6511. https://doi.org/10.1016/j.csbj.2022.11.039.

Heyland, A., Plachetzki, D., Donelly, E., Gunaratne, D., Bobkova, Y., Jacobson, J., Kohn, A.B., Moroz, L.L., 2012. Distinct expression patterns of glycoprotein hormone subunits in the lophotrochozoan Aplysia: implications for the evolution of neuroendocrine systems in animals. Endocrinology 153, 5440–5451. https://doi.org/10.1210/en.2012-1677.

Hsu, S.Y., Nakabayashi, K., Bhalla, A., 2002. Evolution of glycoprotein hormone subunit genes in bilateral metazoa: identification of two novel human glycoprotein hormone subunit family genes, GPA2 and GPB5. J. Mol. Endocrinol. 16, 1538–1551. https://doi.org/10.1210/mend.16.7.0871.

Irachi, S., Hall, D.J., Fleming, M.S., Maugars, G., Björnsson, B.T., Dufour, S., Uchida, K., McCormick, S.D., 2021. Photoperiodic regulation of pituitary thyroid-stimulating hormone and brain deiodinase in Atlantic salmon. Mol. Cell. Endocrinol. 519, 111056. https://doi.org/10.1016/j.mce.2020.111056.

Irisarri, I., Baurain, D., Brinkmann, H., Delsuc, F., Sire, J.-Y., Kupfer, A., Petersen, J., Jarek, M., Meyer, A., Vences, M., Philippe, H., 2017. Phylotranscriptomic consolidation of the jawed vertebrate timetree. Nat. Ecol. Evol. 1, 1370–1378. https://doi.org/10.1038/s41559-017-0240-5.

Jaeschke, H., Schaarschmidt, J., Günther, R., Mueller, S., 2011. The hinge region of the TSH receptor stabilizes ligand binding and determines different signaling profiles of human and bovine TSH. Endocrinology 152, 3986–3996. https://doi.org/10.1210/en.2011-1389.

Jeanne, F., Pilet, S., Klett, D., Combarnous, Y., Bernay, B., Dufour, S., Favrel, P., Sourdaine, P., 2024. Characterization of gonadotropins and their receptors in a chondrichthyan, Scyliorhinus canicula, fills a gap in the understanding of their coevolution. Gen. Comp. Endocrinol. 358, 114614. https://doi.org/10.1016/j.ygcen.2024.114614.

Johansson, M.U., Zoete, V., Michielin, O., Guex, N., 2012. Defining and searching for structural motifs using DeepView/Swiss-PdbViewer. BMC Bioinf. 13, 1–11. https://doi.org/10.1186/1471-2105-13-173.

Male genital ducts and copulatory appendages in chondrichthyans. In: Jones, C.J.P., Walker, T.I., Bell, J.D., Reardon, M.B., Ambrosio, C.E., Almeida, A. (Eds.), 2005. Reproductive Biology and Phylogeny of Chondrichthyes: Sharks, Batoids and Chimaeras. W.C. Hamlett, pp. 371–387. https://doi.org/10.1201/9781439856000-27.

Jones, R.C., Jones, N., Djakiew, D., 1984. Luminal composition and maturation of spermatozoa in the male genital ducts of the Port Jackson shark, *Heterodontus portusjacksoni*. J. Exp. Zool. 230, 417–426. https://doi.org/10.1002/jez.1402300311.

Kenis, S., Istiban, M.N., Van Damme, S., Vandewyer, E., Watteyne, J., Schoofs, L., Beets, I., 2023. Ancestral glycoprotein hormone-receptor pathway controls growth in C. elegans. Front. Endocrinol. 14, 1200407. https://doi.org/10.3389/fendo.2023.1200407.

Kudo, M., Chen, T., Nakabayashi, K., Hsu, S.Y., Hsueh, A.J.W., 2000. The nematode leucine-rich repeat-containing, G protein-coupled receptor (LGR) protein homologous to vertebrate gonadotropin and thyrotropin receptors is constitutively activated in mammalian cells. J. Mol. Endocrinol. 14, 272–284. https://doi.org/10.1210/mend.14.2.0422.

Kumar, R.S., Ijiri, S., Kight, K., Swanson, P., Dittman, A., Alok, D., Zohar, Y., Trant, J.M., 2000. Cloning and functional expression of a thyrotropin receptor from the gonads of a vertebrate (bony fish): potential thyroid-independent role for thyrotropin in reproduction. Mol. Cell. Endocrinol. 167, 1–9. https://doi.org/10.1016/S0303-7207(00)00304-X.

Lemoine, F., Correia, D., Lefort, V., Doppelt-Azeroual, O., Mareuil, F., Cohen-Boulakia, S., Gascuel, O., 2019. NGPhylogeny.fr: new generation phylogenetic services for non-specialists. Nucleic Acids Res. 47, 260–265. https://doi.org/10.1093/nar/gkz303.

Letunic, I., Bork, P., 2021. Interactive Tree of Life (iTOL) v5: an online tool for phylogenetic tree display and annotation. Nucleic Acids Res. 49, 293–296. https://doi.org/10.1093/nar/gkab301.

Levavi-Sivan, B., Bogerd, J., Mañanós, E.L., Gómez, A., Lareyre, J.J., 2010. Perspectives on fish gonadotropins and their receptors. Gen. Comp. Endocrinol. 165, 412–437. https://doi.org/10.1016/j.ygcen.2009.07.019.

Li, C., Habu, Y., Takagi, S., Gotoh, J., Nogimori, T., Hirooka, C., 2004. Distribution of thyrostimulin in the rat: an immunohistochemical study. Endocr. Regul. 37, 223–230. https://doi.org/10.1016/0002-9149(76)90316-7.

Li, H., Zhou, X., Wang, G., Hua, D., Li, S., Xu, T., Dong, M., Cui, X., Yang, X., Wu, Y., Cai, M., Liao, X., Zhang, T., Yang, Z., Du, Y., Li, X., 2022. CAR-T cells targeting TSHR demonstrate safety and potent preclinical activity against differentiated thyroid cancer. J. Clin. Endocrinol. Metab. 107, 1110–1126. https://doi.org/10.1210/clinem/dgab819.

Livak, K.J., Schmittgen, T.D., 2001. Analysis of relative gene expression data using real-time quantitative PCR and the $2-\Delta\Delta CT$ method. Methods 25, 402–408. https://doi.org/10.1006/meth.2001.1262.

Loir, M., Sourdaine, P., 1994. Testes cells: isolation and culture. In: Hochachka, P.W., Mommsen, T.P. (Eds.), Biochemistry and Molecular Biology of Fishes: Analytical Techniques, pp. 219–272. New York.

Lutton, B.V., Callard, I.P., 2007. Effects of reproductive activity and sex hormones on apoptosis in the epigonal organ of the skate (Leucoraja erinacea). Gen. Comp. Endocrinol. 154, 75–84. https://doi.org/10.1016/j.ygcen.2007.06.014.

Marra, N.J., Stanhope, M.J., Jue, N.K., Wang, M., Sun, Q., Pavinski Bitar, P., Richards, V. P., Komissarov, A., Rayko, M., Kliver, S., Stanhope, B.J., Winkler, C., O'Brien, S.J., Antunes, A., Jorgensen, S., Shivji, M.S., 2019. White shark genome reveals ancient elasmobranch adaptations associated with wound healing and the maintenance of genome stability. Proc. Natl. Acad. Sci. USA 116, 4446–4455. https://doi.org/10.1073/pnas.1819778116.

Maugars, G., Dufour, S., Cohen-Tannoudji, J., Quérat, B., 2014. Multiple thyrotropin β-subunit and thyrotropin receptor-related genes arose during vertebrate evolution. PLoS One 9, e111361. https://doi.org/10.1371/journal.pone.0111361.

Mueller, S., Kleinau, G., Szkudlinski, M.W., Jaeschke, H., Krause, G., Paschke, R., 2009. The superagonistic activity of bovine thyroid-stimulating hormone (TSH) and the human TR1401 TSH analog is determined by specific amino acids in the hinge region of the human TSH receptor. JBC 284, 16317–16324. https://doi.org/10.1074/jbc.M109.005710.

Nagasaki, H., Wang, Z., Jackson, V.R., Lin, S., Nothacker, H.P., Civelli, O., 2006. Differential expression of the thyrostimulin subunits, glycoprotein α2 and β5 in the rat pituitary. J. Mol. Endocrinol. 37, 39–50. https://doi.org/10.1677/jme.1.01932.

Nakabayashi, K., Matsumi, H., Bhalla, A., Bae, J., Mosselman, S., Hsu, S.Y., Hsueh, A.J. W., 2002. Thyrostimulin, a heterodimer of two new human glycoprotein hormone subunits, activates the thyroid-stimulating hormone receptor. J. Clin. Investig. 109, 1445–1452. https://doi.org/10.1172/JCI0214340.

Okada, S.L., Ellsworth, J.L., Durnam, D.M., Haugen, H.S., Holloway, J.L., Kelley, M.L., Lewis, K.E., Ren, H., Sheppard, P.O., Storey, H.M., Waggie, K.S., Wolf, A.C., Yao, L. Y., Webster, P.J., 2006. A glycoprotein hormone expressed in corticotrophs exhibits unique binding properties on thyroid-stimulating hormone receptor. Mol. Endocrinol. 20, 414–425. https://doi.org/10.1210/me.2005-0270.

Okajima, Y., Nagasaki, H., Suzuki, C., Suga, H., Ozaki, N., Arima, H., Hamada, Y., Civelli, O., Oiso, Y., 2008. Biochemical roles of the oligosaccharide chains in thyrostimulin, a heterodimeric hormone of glycoprotein hormone subunits alpha2 (GPA2) and beta5 (GPB5). Regul. Pept. 148, 62–67. https://doi.org/10.1016/j.regpep.2008.03.002.

Piferrer, F.C., Callard, G.V., 1995. Inhibition of deoxyribonucleic acid synthesis during premeiotic stages of spermatogenesis by a factor from testis-associated lymphomyeloid tissue in the dogfish shark (Squalus acanthias). Biol. Reprod. 53, 390–398. https://doi.org/10.1095/biolreprod53.2.390.

Pudney, J., Callard, G.V., 1984b. Development of agranular reticulum in Sertoli cells of the testis of the dogfishSqualus acanthias during spermatogenesis. Anat. Rec. 209, 311–321. https://doi.org/10.1002/ar.1092090309.

Pudney, J., Callard, G.V., 1984a. Identification of Leydig-like cells in the testis of the dogfish Squalus acanthias. Anat. Rec. 209, 323–330. https://doi.org/10.1002/ar.1092090310.

Querat, B., 2021. Unconventional actions of glycoprotein hormone subunits: a comprehensive review. Front. Endocrinol. 12, 731966. https://doi.org/10.3389/fendo.2021.731966.

Read, T.D., Petit, R.A., Joseph, S.J., Alam, MdT., Weil, M.R., Ahmad, M., Bhimani, R., Vuong, J.S., Haase, C.P., Webb, D.H., Tan, M., Dove, A.D.M., 2017. Draft sequencing and assembly of the genome of the world's largest fish, the whale shark: Rhincodon typus Smith 1828. BMC Genom. 18, 532. https://doi.org/10.1186/s12864-017-3926-9.

Redon, E., Bosseboeuf, A., Rocancourt, C., Da Silva, C., Wincker, P., Mazan, S., Sourdaine, P., 2010. Stage-specific gene expression during spermatogenesis in the dogfish (Scyliorhinus canicula). Reproduction 140, 57–71. https://doi.org/10.1530/REP-10-0021.

Rocco, D.A., Garcia, A.S.G., Scudeler, E.L., dos Santos, D.C., Nóbrega, R.H., Paluzzi, J.-P. V., 2019. Glycoprotein hormone receptor knockdown leads to reduced reproductive success in male Aedes aegypti. Front. Physiol. 10, 266. https://doi.org/10.3389/fphys.2019.00266.

Rocco, D.A., Kim, D.H., Paluzzi, J.-P.V., 2017. Immunohistochemical mapping and transcript expression of the GPA2/GPB5 receptor in tissues of the adult mosquito, Aedes aegypti. Cell Tissue Res. 369, 313–330. https://doi.org/10.1007/s00441-017-2610-3.

Rocco, D.A., Paluzzi, J.-P.V., 2020. Expression profiling, downstream signaling, and inter-subunit interactions of GPA2/GPB5 in the adult mosquito Aedes aegypti. Front. Endocrinol. 11, 158. https://doi.org/10.3389/fendo.2020.00158.

Roch, G.J., Sherwood, N.M., 2014. Glycoprotein hormones and their receptors emerged at the origin of metazoans. GBE 6, 1466–1479. https://doi.org/10.1093/gbe/evu118.

Rocha, A., Gómez, A., Galay-Burgos, M., Zanuy, S., Sweeney, G.E., Carrillo, M., 2007. Molecular characterization and seasonal changes in gonadal expression of a thyrotropin receptor in the European sea bass. Gen. Comp. Endocrinol. 152, 89–101. https://doi.org/10.1016/j.ygcen.2007.03.001.

Schefe, J.H., Lehmann, K.E., Buschmann, I.R., Unger, T., Funke-Kaiser, H., 2006. Quantitative real-time RT-PCR data analysis: current concepts and the novel "gene expression's C T difference" formula. J. Mol. Med. 84, 901–910. https://doi.org/10.1007/s00109-006-0097-6.

Schwartz, J., Réalis-Doyelle, E., Le Franc, L., Favrel, P., 2021. A novel dop2/invertebrate-type dopamine signaling system potentially mediates stress, female reproduction, and early development in the pacific oyster (Crassostrea gigas). Mar. Biotechnol. 683–694. https://doi.org/10.1007/s10126-021-10052-5.

Sievers, F., Wilm, A., Dineen, D., Gibson, T.J., Karplus, K., Li, W., Lopez, R., McWilliam, H., Remmert, M., Söding, J., Thompson, J.D., Higgins, D.G., 2011. Fast, scalable generation of high-quality protein multiple sequence alignments using Clustal Omega. Mol. Syst. Biol. 7, 539. https://doi.org/10.1038/msb.2011.75.

Sourdaine, P., Garnier, D.H., 1993. Stage-dependent modulation of Sertoli cell steroid production in dogfish (Scyliorhinus canicula). Reproduction 97, 133–142. https://doi.org/10.1530/jrf.0.0970133.

Sower, S.A., Decatur, W.A., Hausken, K.N., Marquis, T.J., Barton, S.L., Gargan, J., Freamat, M., Wilmot, M., Hollander, L., Hall, J.A., Nozaki, M., Shpilman, M., Levavi-Sivan, B., 2015. Emergence of an ancestral glycoprotein hormone in the pituitary of the sea lamprey, a basal vertebrate. Endocrinology 156, 3026–3037. https://doi.org/10.1210/en.2014-1797.

Sower, S.A., Hausken, K.N., 2017. A lamprey view on the origins of neuroendocrine regulation of the thyroid axis. Mol. Cell. Endocrinol. 459, 21–27. https://doi.org/10.1016/j.mce.2017.04.012.

Studer, G., Rempfer, C., Waterhouse, A.M., Gumienny, R., Haas, J., Schwede, T., 2020. QMEANDisCo—distance constraints applied on model quality estimation. Bioinformatics 36, 1765–1771. https://doi.org/10.1093/bioinformatics/btz828.

Sudo, S., Kuwabara, Y., Park, J.-I., Hsu, S.Y., Hsueh, A.J.W., 2005. Heterodimeric fly glycoprotein hormone-α2 (GPA2) and glycoprotein hormone-β5 (GPB5) activate fly leucine-rich repeat-containing G protein-coupled receptor-1 (DLGR1) and stimulation of human thyrotropin receptors by chimeric fly GPA2 and human GPB5. Endocrinology 146, 3596–3604. https://doi.org/10.1210/en.2005-0317.

Sullivan, R., Saez, F., Girouard, J., Frenette, G., 2005. Role of exosomes in sperm maturation during the transit along the male reproductive tract. Blood Cells Mol. Dis. 35, 1–10. https://doi.org/10.1016/j.bcmd.2005.03.005.

Sun, S.-C., Hsu, P.-J., Wu, F.-J., Li, S.-H., Lu, C.-H., Luo, C.-W., 2010. Thyrostimulin, but not thyroid-stimulating hormone (TSH), acts as a paracrine regulator to activate the TSH receptor in mammalian ovary. J. Biol. Chem. 285, 3758–3765. https://doi.org/10.1074/jbc.M109.066266.

Suzuki, C., Nagasaki, H., Okajima, Y., Suga, H., Ozaki, N., Arima, H., Iwasaki, Y., Oiso, Y., 2009. Inflammatory cytokines regulate glycoprotein subunit β5 of thyrostimulin through nuclear factor-κB. Endocrinology 150, 2237–2243. https://doi.org/10.1210/en.2008-0823.

Ulloa-Aguirre, A., Zariñán, T., Jardón-Valadez, E., Gutiérrez-Sagal, R., Dias, J.A., 2018. Structure-function relationships of the follicle-stimulating hormone receptor. Front. Endocrinol. 9, 707. https://doi.org/10.3389/fendo.2018.00707.

Vandersmissen, H.P., Van Hiel, M.B., Van Loy, T., Vleugels, R., Vanden Broeck, J., 2014. Silencing D. melanogaster lgr1 impairs transition from larval to pupal stage. Gen. Comp. Endocrinol. 209, 135–147. https://doi.org/10.1016/j.ygcen.2014.08.006.

Wahl, M., Levy, T., Manor, R., Aflalo, E.D., Sagi, A., Aizen, J., 2022. Genes encoding the glycoprotein hormone GPA2/GPB5 and the receptor LGR1 in a female prawn. Front. Endocrinol. 13, 823818. https://doi.org/10.3389/fendo.2022.823818.

Wang, P., Liu, S., Yang, Q., Liu, Z., Zhang, S., 2018. Functional characterization of thyrostimulin in amphioxus suggests an ancestral origin of the TH signaling pathway. Endocrinology 159, 3536–3548. https://doi.org/10.1210/en.2018-00550.

Wang, Q., Arighi, C.N., King, B.L., Polson, S.W., Vincent, J., Chen, C., Huang, H., Kingham, B.F., Page, S.T., Farnum Rendino, M., Thomas, W.K., Udwary, D.W., Wu, C.H., the North East Bioinformatics Collaborative Curation Team, 2012. Community annotation and bioinformatics workforce development in concert - little skate genome annotation workshops and jamborees. Database. https://doi.org/10.1093/database/bar064, 2012, bar064.

Waterhouse, A., Bertoni, M., Bienert, S., Studer, G., Tauriello, G., Gumienny, R., Heer, F. T., de Beer, T.A.P., Rempfer, C., Bordoli, L., Lepore, R., Schwede, T., 2018. SWISS-MODEL: homology modelling of protein structures and complexes. Nucleic Acids Res. 46, 296–303. https://doi.org/10.1093/nar/gky427.

Yang, L.-K., Zhang, J., Liu, D., Han, T.-Y., Qin, Q.-S., Wang, A.-Q., Dong, B., 2023. Ancestral glycoprotein hormone and its cognate receptor present in primitive chordate ascidian: molecular identification and functional characterization. Int. J. Biol. Macromol. 229, 401–412. https://doi.org/10.1016/j.ijbiomac.2022.12.297.

Ye, J., Coulouris, G., Zaretskaya, I., Cutcutache, I., Rozen, S., Madden, T.L., 2012. Primer-BLAST: a tool to design target-specific primers for polymerase chain reaction. BMC Bioinf. 13, 1–11. https://doi.org/10.1186/1471-2105-13-134.

Yoshimura, T., 2010. Neuroendocrine mechanism of seasonal reproduction in birds and mammals. Anim. Sci. J. 81, 403–410. https://doi.org/10.1111/j.1740-0929.2010.00777.x.

Zhang, M., Wei, H., Liu, T., Li, W., Li, Y., Wang, S., Xing, Q., Hu, X., Zhang, L., Bao, Z., 2020. Potential GnRH and steroidogenesis pathways in the scallop Patinopecten yessoensis. J. Steroid Biochem. Mol. Biol. 204, 105756. https://doi.org/10.1016/j.jsbmb.2020.105756.